Title:

Hyperactive MEK1 signaling in cortical GABAergic interneurons causes embryonic parvalbumin-neuron death and deficits in behavioral inhibition.

Authors:

Michael C. Holter[1], Lauren T. Hewitt[1,#], Kenji J. Nishimura[1,#], George R. Bjorklund[1], Shiv Shah[1], Noah R. Fry[1], Katherina P. Rees[1], Tanya A. Gupta[2], Carter W. Daniels[2,†], Guohui Li[3], Steven Marsh[4], David M. Treiman[4], M. Foster Olive[2], Trent R. Anderson[3], Federico Sanabria[2], William D. Snider[5], Jason M. Newbern[1,*]

Affiliations:

[1]School of Life Sciences, [2]Department of Psychology, Arizona State University; Tempe, AZ 85287, USA

[3]College of Medicine, University of Arizona; Phoenix, AZ 85004, USA

[4]Barrow Neurological Institute; Phoenix, AZ 85013, USA

[5]University of North Carolina Neuroscience Center, The University of North Carolina School of Medicine; Chapel Hill, NC, 27599, USA

[#]Present Address: Interdepartmental Neuroscience Graduate Program, University of Texas; Austin, TX, 78712, USA

[†]Present Address: Department of Psychiatry, Columbia University, New York, NY 10032, USA

*Lead Contact/Corresponding Author address:

School of Life Sciences, PO Box 84501

Arizona State University

Tempe, AZ 85287-4501, USA

*Correspondence: jason.newbern@asu.edu

Highlights

- GABAergic-specific MEK1 hyperactivation causes immature parvalbumin neuron death
- Deletion of *Erk1/2* has no effect on cortical interneuron number
- Increased MEK1 activity leads to perineuronal net growth and seizure-like activity
- Behavioral inhibition is disrupted by MEK1 hyperactivation in GABAergic circuits

Summary

Abnormal ERK/MAPK pathway activity is a contributor to multiple neurodevelopmental disorders, especially the RASopathies, which are associated with intellectual disability, ADHD, autism, and epilepsy. Here, we examined whether ERK/MAPK signaling regulates the development of GABAergic cortical interneurons (CINs), a heterogeneous population of inhibitory neurons necessary for cortical function. We show that ERK1/2 is not required for the initial establishment of CIN number. However, hyperactivation of MEK1 leads to increased caspase-3 activation in the embryonic subpallium and a selective loss of mature parvalbumin-expressing (PV) CINs. Surviving mutant PV-CINs have a typical fast-spiking phenotype but display a robust increase in perineuronal net accumulation. Hyperactive MEK1 mutant mice exhibit seizure-like phenotypes and a reduction in perisomatic inhibitory synapses. We also detected altered PFC development and impaired behavioral response inhibition in mutants. Our data suggests PV-CIN development is particularly sensitive to hyperactive MEK1 signaling which may underlie neurological phenotypes frequently observed in ERK/MAPK-linked syndromes.

Keywords

ERK1/2, cerebral cortex, development, ganglionic eminence, ADHD, RASopathy, kinase, apoptosis, response inhibition capacity

Introduction

Multiple developmental disorders are caused by genetic mutations linked to perturbation of kinase activity and altered intracellular signaling. The RAS/RAF/MEK/ERK (ERK/MAPK) pathway is a well-known, ubiquitous signaling cascade that is dynamically activated during development (Krens et al., 2006; Samuels et al., 2009). Mutations in classic RAS/MAPK signaling pathway components or upstream regulators, such as *PTPN11/SHP2*, *NF1*, or *SYNGAP1*, cause a family of related syndromes, known collectively as the RASopathies (Tidyman and Rauen, 2016). Moreover, *MAPK3/ERK1* is present in a frequently mutated region of 16p11.2 linked to Autism Spectrum Disorder (ASD) and animal models of Fragile X, Rett, and Angelmann Syndromes also exhibit changes in ERK/MAPK signaling activity (Kumar et al., 2008; Pucilowska et al., 2015; Vorstman et al., 2006). These disorders are often associated with intellectual disability, neurodevelopmental delay, ADHD, autism, and epilepsy. Clearly, aberrant ERK/MAPK activity is an important molecular mediator of neurodevelopmental abnormalities, however, therapeutic approaches for these conditions are lacking, due in part to a limited understanding of the developmental stage- and cell-specific functions of ERK/MAPK signaling in the brain. Delineating the precise consequences of altered ERK/MAPK activity on specific neuronal subtypes in the developing forebrain may provide insight into the neuropathogenesis of multiple neurodevelopmental diseases.

Coordinated interactions between multiple cell types are necessary for normal brain function, but deficits in select cellular subtypes often mediate specific neurodevelopmental phenotypes. Past work has shown that ERK/MAPK signaling regulates the development of dorsal cortex-derived glutamatergic cortical projection neurons (PNs) and glia (Aoidi et al., 2018; Ehrman et al., 2014; Ishii et al., 2013; Li et al., 2012). Upstream regulators, such as *Syngap1*, are also crucial for the early development of cortical glutamatergic neuron structure, excitability, and cognition (Clement et al., 2012; Ozkan et al., 2014). In contrast, NF1 mutations have been shown to impair aspects of spatial learning and memory via disruption of GABAergic, but not glutamatergic, neuron function (Cui et al 2008). Abnormal GABAergic circuitry is thought to be a key feature in the neuropathogenesis of various other neurodevelopmental disorders (Chao et al., 2010; Cui et al., 2008; Paluszkiewicz et al., 2011; Zhang et al., 2010). GABAergic neuron-directed

Syngap1 loss modulates GABAergic output but does not drive major abnormalities in mouse behavior or seizure threshold (Berryer et al., 2016; Ozkan et al., 2014). Mutations in signaling components upstream of *Ras* differentially modulate multiple downstream pathways and do not provide a clear delineation of ERK/MAPK function (Anastasaki and Gutmann, 2014; Brown et al., 2012). Here, we have selectively altered the activation of downstream kinases, MEK1 and ERK1/2, to definitively examine the precise functions of the core ERK/MAPK cascade in the development of GABAergic cortical interneurons (CINs).

In the mature cortex, locally connected parvalbumin- (PV) and somatostatin-expressing (SST) CINs comprise the most populous and functionally diverse GABAergic subtypes (Kessaris et al., 2014). Reduced PV-CIN number is often observed in mouse models of multiple neurodevelopmental diseases, however, the mechanism of loss is poorly understood (Chao et al., 2010; Cui et al., 2008; Steullet et al., 2017). PV- and SST-CINs are generated in spatiotemporal fashion primarily from the medial ganglionic eminence (MGE) and migrate tangentially to the cortical plate (Gelman et al., 2009; Gelman and Marín, 2010; Lavdas et al., 1999; Marin and Rubenstein, 2001, 2003; Parnavelas, 2000; Tamamaki et al., 1997; Wichterle et al., 1999; Wichterle et al., 2001; Wonders and Anderson, 2006). Tangential migration and early GABAergic circuit development is regulated by BDNF/TRKB, GDNF/GFRα1, HGF/MET, and NRG/ERBB4 signaling, which activate multiple Receptor Tyrosine Kinase (RTK)-linked intracellular kinase cascades, including ERK/MAPK (Bae et al., 2010; Fazzari et al., 2010; Flames et al., 2004; Perrinjaquet et al., 2011; Pozas and Ibanez, 2005). While the transcriptional basis of GABAergic neuron development has been well-studied (Lim et al., 2018; Mayer et al., 2018; Mi et al., 2018; Paul et al., 2017), the kinase cascades that mediate GABAergic development in response to critical extracellular cues have received less attention.

We therefore examined the basic requirements and pathological contributions of ERK/MAPK signaling to CIN development. We show that ERK1/2 is not required for the early establishment of CIN number. In contrast, GABAergic-specific overexpression of constitutively-active MEK1 (caMEK1) resulted in caspase-3 activation in a subset of embryonic GABAergic neurons. Even though caMEK1 is expressed in all CINs, we only observed a significant reduction in the number of PV-CINs, but not SST-

CINs. In contrast with past models exhibiting PV-CIN loss, we found a surprising increase in the extent of perineuronal net (PNN) accumulation around these cells (Steullet et al., 2017). We also observed an increased risk of spontaneous epileptiform activity and mild seizure-like activity in a subset of mutant mice that coincides with a reduction in inhibitory synapses on pyramidal neurons. Mutant mice exhibited normal locomotor, anxiety-like, and social behaviors, but we noted deficits in behavioral response inhibition capacity, a process linked to ADHD-like phenotypes. Our findings indicate that GABAergic-specific MEK1 hyperactivation is sufficient to drive widespread changes in cortical development relevant to cognitive phenotypes observed in RASopathies. Together, these data define the precise functions of ERK/MAPK signaling in CIN development and suggest preferential contributions of PV-CIN pathology to ERK/MAPK-linked disorders.

Results

Differential expression of ERK/MAPK components in CINs

The ERK/MAPK cascade is a commonly utilized intracellular signaling pathway that is dynamically activated during embryogenesis and in adulthood. In the embryonic ventricular zone, neural progenitors typically show high levels of P-ERK1/2 relative to immature post-mitotic neurons (Pucilowska et al., 2018; Stanco et al., 2014). In adult cortices, elevated P-ERK1/2 labeling is enriched in a heterogeneous set of excitatory PNs, primarily in layer 2, and plays a critical role in long-range PN development (Cancedda et al., 2003; Gauthier et al., 2007; Holter et al., 2019; Pham et al., 2004; Pucilowska et al., 2012; Suzuki et al., 2004; Xing et al., 2016). The activation of ERK1/2 in CINs has not been well characterized. We generated mice expressing *Slc32A1:Cre* and the Cre-dependent red fluorescent protein (RFP) reporter, *Ai9* (Madisen et al., 2010; Vong et al., 2011) (Figure1A-D) . As expected, brain regions abundant with GABA-expressing neurons robustly expressed *Ai9* (Figure 1A). Immunolabeling for MAP2K1 (MEK1) revealed relatively lower expression in CINs in comparison to $NeuN^{+}/RFP^{-}$ presumptive PNs (Figure 1E-G). Layer II/III CINs also expressed low levels of MAPK1/ERK2 in comparison to PNs (Figure 1H-J). In agreement with previous studies, high levels of P-ERK1/2 were observed in a subset of

PNs in cortical layer II/III (Cancedda et al., 2003; Pham et al., 2004; Suzuki et al., 2004). However, examination of P-ERK1/2 immunolabeling in RFP^+ CINs revealed qualitatively lower levels of P-ERK1/2 in comparison to PNs (Figure 1K-M). In summary, CINs express relatively lower levels of MEK1, ERK2, and P-ERK1/2 than excitatory neurons in the adult cortex, raising the possibility of functionally distinct roles for this cascade between these two primary cortical neuron subtypes.

GABAergic-autonomous caMEK1 expression decreases PV-CIN number

Increased ERK/MAPK signaling is the most common result of RASopathy-linked mutations (Tidyman and Rauen, 2016). We utilized a Cre-dependent, constitutively active *CAG-Loxp-Stop-Loxp-Mek1*$^{S217/221E}$ (*caMek1*) allele, which has been shown to hyperactivate MEK1/2-ERK1/2 signaling (Alessi et al., 1994; Bueno et al., 2000; Cowley et al., 1994; Klesse et al., 1999; Krenz et al., 2008; Lajiness et al., 2014; Li et al., 2012). We generated *caMek1*, *Slc32A1:Cre* mice to hyperactivate MEK1 in a CIN-specific fashion during embryogenesis. Elevated MEK1 expression was clearly detectable in the E13.5 mantle zone of the ganglionic eminences, presumptive embryonic CINs migrating into the cortex, and adult CINs in primary somatosensory cortex (S1) (Figure S1A-H; J-O). *CaMek1*, *Slc32A1:Cre* mice were viable and phenotypically normal, though mutants exhibited larger body mass than controls in adulthood (Figure S1I).

Surprisingly, assessment of fluorescently-labeled CINs in *caMek1*, *Slc32A1:Cre*, *Ai9* sensory cortices revealed a significant reduction in total RFP^+ cell density (Figure 2A-I). In the adult cortex, approximately 40% of CINs express PV whereas 30% express SST, which serve as mostly non-overlapping markers of two distinct populations of CINs (Kelsom and Lu, 2013; Kessaris et al., 2014; Rudy et al., 2011). Strikingly, we observed a significant reduction in the proportion of PV^+/RFP^+ CINs, but not in the proportion of SST^+/RFP^+ CINs (Figure 2K-Q). PV, but not SST, expressing CINs displayed a significant increase in somal area compared to control neurons (Figure 2R-U, V). A reduced density of PV-CINs was detected in a separate *caMek1, Dlx5/6:Cre* strain that also targets postmitotic CINs in the developing cortex (Figure S2A-D) (Monory et al., 2006).

Recombination within the entire GABAergic system raises the possibility that indirect changes in other neuroanatomical regions could alter global cortical activity and modulate PV-CIN number (Denaxa et al., 2018). To restrict Cre expression to primarily MGE-derived CINs, we generated *caMek1*, *Nkx2.1:Cre* mice and assessed the proportion of PV^+/RFP^+ CINs. *CaMek1*, *Nkx2.1:Cre* mice exhibited generalized growth delay in the second-third postnatal week and were not viable past the first postnatal month (n=8). Nonetheless, consistent with our previous findings, P14 *caMek1*, *Nkx2.1:Cre, Ai9* mice displayed a reduction in PV^+/RFP^+-CIN density (Figure S2E-L, M). In summary, our data indicate that the establishment of PV-CIN number is cell-autonomously vulnerable to enhanced MEK1 signaling, while SST-CIN number is not altered.

Reduced ERK/MAPK signaling does not alter CIN density

ERK/MAPK activity is necessary for the survival and physiological maturation of select dorsal cortex-derived PNs (Li et al., 2012; Xing et al., 2016), but it is unclear if ERK/MAPK is necessary for the establishment of CIN number *in vivo*. We therefore generated quadruple transgenic mice that express germline *Mapk3/Erk1*$^{-/-}$ null alleles (*Erk1*$^{-/-}$), conditional inactivating *Mapk1*/*Erk2* alleles (*Erk2*$^{fl/fl}$), *Slc32A1:Cre*$^{+/-}$, and *Ai9*$^{+/-}$ (Newbern et al., 2009; Xing et al., 2016). *Erk1*$^{-/-}$, *Erk2*$^{fl/fl}$, *Slc32A1:Cre, Ai9* mice were born at normal Mendelian ratios, but exhibited profound growth delay by the end of the first postnatal week and lethality in the second to third postnatal week (n=10). No gross neuroanatomical abnormalities between mutant and control forebrains were observed in the first postnatal week (Figure 3A-B). ERK2 immunolabeling confirmed a reduction of ERK2 protein in mutant CINs in layer 5 in comparison to controls (Figure 3C-H). Surprisingly, no significant difference in the relative density of RFP^+ CINs was observed between mutant and control cortices (Figure 3I-L, M). Similar results were obtained in *Erk1*$^{-/-}$, *Erk2*$^{fl/fl}$, *Dlx5/6:Cre, Ai3* mice (Supplemental Figure 3A-D). Early growth delay and lethality limited further assessment of GABAergic maturation and subtype specification. Nonetheless, these data reveal that ERK/MAPK signaling is dispensable for the establishment of CIN number through the first postnatal week.

Presumptive PV-CINs in the embryonic subpallium undergo cleaved caspase 3-mediated apoptosis

CIN number is refined by activity-dependent programmed cell death at the end of the first postnatal week (Southwell et al., 2012). However, our analyses of RFP^+ CINs in P3.5 S1 yielded a significant reduction in CIN density. We therefore hypothesized that gain-of-function MEK1 signaling disrupted embryonic processes necessary to establish CIN number. Indeed, examination of RFP^+ CIN density in the E17.5 cortical plate also revealed fewer CINs in *caMek1, Slc32A1:Cre* embryos (Figure S4A-D). Thus, we examined the possibility of CIN death during mid-neurogenesis in the *caMek1, Slc32A1:Cre, Ai9* subpallium. Immunolabeling for the apoptotic marker cleaved caspase 3 (CC3) revealed colocalization of CC3 with some RFP^+ neurons within the mantle zone of the ganglionic eminences in E13.5 mutant, but not control, embryos (Figure 4A-E, F). $CC3^+/RFP^+$ neurons also presented with condensed, pyknotic nuclei (Figure 4G-N). We also observed $CC3^+/RFP^+$ cells with pyknotic nuclei in *caMek1*, *Nkx2.1:Cre, Ai9* mantle zone (Figure 4O-Q). No apoptotic cells were observed in the mutant ganglionic eminence VZ or the cortical migratory streams (data not shown). Analysis of recombined GABAergic neuron density in the dorsal striatum did not reveal a significant difference from controls, suggesting that the loss of PV-CINs is not due to altered CIN migratory trajectory (data not shown). Together, our results suggest reduced PV-CIN density in the postnatal cortex is due to the death of a subset of migrating CINs in the ganglionic eminence.

GABAergic-specific caMek1 promotes cortical hyperexcitability but does not significantly alter fast-spiking CIN electrophysiological properties

As many as 40% of RASopathy individuals experience seizures and epilepsy is prominent in individuals with mutations downstream of *Ras* (Digilio et al., 2011; Rauen et al., 2013; Yoon et al., 2007). Whether MEK1 hyperactivation in GABAergic circuits mediates seizure activity in the RASopathies has not been explored. We did not detect any signs of overt generalized tonic-clonic seizures while housed in home cages. We conducted a series of behavioral tests by first using the open field, then the elevated plus maze, and finally the social approach assay. No difference in global locomotor activity, anxiety-like behavior, or sociability could be detected in these tests (Figure S5). However, during the initial 60 sec of

open field testing with 13 adult *caMek1, Slc32A1:Cre* mutants, two mutant mice exhibited increased head twitching, aberrant locomotor activity, and increased rearing (Supp. Video 1) and three mutant mice displayed periods of overt sudden behavioral arrest and motionless staring (Supp Video 2). These behaviors were not observed in any of the control mice utilized in this study. Consistent with these subtle impairments, subsequent re-analysis of the first 10 sec of the open field task revealed a significant reduction in distance traveled in *caMek1, Slc32A1:Cre* mutants, which was also observed in *caMek1, Dlx5/6:Cre* mutants (data not shown).

We performed intracortical EEG recordings to directly assess cortical activity, which revealed spontaneous epileptiform-like discharges in three of six *caMek1, Slc32A1:Cre* adult mice, but not control mice (Figure 5A). These six mutants also exhibited a significantly reduced threshold to seizure induction in response to pentylenetetrazol (PTZ) administration when compared to controls (Figure 5B). Seizures have been shown to increase the local expression of glial fibrillary acidic protein (GFAP) in astrocytes (Steward et al., 1992; Stringer, 1996). Indeed, 3 of 3 newly generated and untreated *caMek1 Slc32A1:Cre* mice immunolabeled for GFAP exhibited clusters of GFAP-expressing astrocytes in the cortex consistent with local reactive astrogliosis near hyperexcitable regions (Figure 5C-F). Overall, many of the seizure-related phenotypes we observed were not completely penetrant, thus, these data indicate that MEK1 hyperactivation in CINs may be a potential risk factor for epilepsy in the RASopathies.

PV-CINs provide a powerful source of inhibition in the cortex, firing action potentials at frequencies greater than 200Hz (Okaty et al., 2009). Fast-spiking (FS) physiology is due in part to the unique expression of the fast-inactivating potassium channel Kv3.1, which begins in the second postnatal week (Goldberg et al., 2011; Rosato-Siri et al., 2015; Rudy and McBain, 2001). To determine if hyperactive MEK1 signaling was sufficient to alter basic physiological properties of FS CINs, we performed whole-cell patch clamp recordings on *caMek1*, *Nkx2.1:Cre* mice at the end of the third postnatal week. Current clamp recordings of fluorescently-labeled CINs revealed that both control and mutant neurons retained their distinctive electrophysiological fast-spiking phenotype (Figure 5G, I) (Agmon & Connors, 2018; Anderson et al., 2010; McCormick et al., 1985). No significant differences were observed in resting membrane

potential, adaptation index, rheobase, or action potential threshold, but a small increase in action potential amplitude was observed (Figure 5I). We did also detect a significant increase in FS CIN input resistance and a reduction in FI slope in *caMek1*, *Nkx2.1:Cre* mutant compared with *Nkx2.1:Cre* controls suggesting that mutants may have a reduction in the responsiveness and/or firing output of inhibitory neurons (Figure 5H-I). Overall, these data indicate that canonical electrophysiological features of fast-spiking CIN development were not altered by MEK1 hyperactivation. However, certain intrinsic properties exhibit subtle differences in mutant mice that might contribute to circuit-wide hyperexcitability.

Reduced perisomatic GABAergic innervation of layer 2/3 pyramidal neuron cell soma

PV-expressing CINs preferentially innervate pyramidal cells, where synaptic targets are dependent on PV-CIN morphology (Chattopadhyaya et al., 2004; Chattopadhyaya et al., 2007). Basket cells often innervate the PN soma, whereas chandelier cells target the PN axon initial segment (Chattopadhyaya et al., 2004; Chattopadhyaya et al., 2007; Fino et al., 2013). We examined perisomatic VGAT-expressing synapses surrounding layer 2/3 PNs in adult *caMek1*, *Slc32A1:Cre, Ai3* mice. We found the extent of VGAT-immunolabeling in the perisomatic space of $NeuN^{+}/GFP^{-}$ PN soma was significantly reduced in mutant cortices when compared to controls (Fig. 6A-F, K). Interestingly, the area of VGAT-labeling in the surrounding neuropil, typically innervated by SST-CINs, was unchanged (Fig. 6G-J, K). These data show that PV-CIN inhibitory output is selectively vulnerable to caMEK1 signaling while SST-CINs are less affected.

Surviving PV-CINs exhibit enhanced perineuronal net accumulation

PV-CINs selectively accumulate an extracellular structure called the perineuronal net (PNN) derived primarily from glial chondroitin sulfate proteoglycans (CSPGs). PNNs are essential to cortical development, marking the closure of critical periods and protecting PV-CINs from the high level of oxidative stress associated with a high frequency firing rate (Cabungcal et al., 2013; Hensch, 2005b). Reductions in PNN formation have been noted in multiple models of neurodevelopmental disorders, many

of which also exhibit a coincident loss of PV-CINs (Bitanihirwe and Woo, 2014; Cabungcal et al., 2013; Krencik et al., 2015; Krishnan et al., 2015; Steullet et al., 2017).

We utilized WFA-labeling to study PNN formation in adult *caMek1*, *Slc32A1:Cre, Ai3* mice (Figure 7A-F). We found that all surviving PV-CINs were WFA^+ in mutants; PNNs were not detected on *Ai3*-expressing neurons that lacked PV-expression. Analysis of the quantitative level of WFA-labeling in mutant PV-CINs revealed a robust increase in PNN accumulation as compared to controls (Figure 7C-F, H). In agreement with the larger somal size of mutant PV-CINs, the cross-sectional area of WFA-labeled profiles was significantly increased (Figure 7G). Interestingly, mutant WFA-labeled CINs exhibited normal expression of 8-oxo-2'-deoxyguanosine (8-oxo-dg), a marker of DNA oxidation often altered in neurons with reduced PNNs (Figure 7I-L) (Steullet et al., 2017). Collectively, MEK1 hyperactivation does not trigger PNN formation on GABAergic neurons lacking PV, but clearly increases PNN accumulation.

caMek1, Slc32A1:Cre mice display delayed acquisition of FMI performance

Attention deficit hyperactivity disorder (ADHD) is a major co-morbid condition associated with a significant proportion of RASopathy cases (Adviento et al., 2014; Garg et al., 2013; Green et al., 2017; Pierpont et al., 2018; Walsh et al., 2013). Inappropriate prefrontal cortex (PFC) function has been implicated in ADHD (Gabay et al., 2018), and has been shown to contribute to cognitive deficits in a mouse model of Fragile X Syndrome (Krueger et al., 2011). Few studies have examined GABAergic contributions to PFC function, particularly in the context of RASopathies. As in sensory cortex, we noted a reduction in *Ai9*-expressing CINs in the PFC of mutant mice (Figure 8A-B, D-E). Interestingly, we found that PNs in the PFC exhibit reduced P-ERK1/2 expression in *caMek1, Slc32A1:Cre* mice (Figure 8A-F). These data indicate that MEK1 hyperactivation in developing CINs is sufficient to drive molecular abnormalities within specific cortical regions important for cognition.

Individuals with ADHD often exhibit structural changes in the PFC, which appear to be involved in the inhibition of reinforced responses (Seidman et al., 2006). To examine response inhibition directly, we utilized a fixed minimum interval (FMI) test, a timing-based task that requires animals to withhold a

response for a fixed period. This paradigm is perhaps more favorable than the five-choice serial reaction time task (5-CSRTT) and differential reinforcement of low rates task (DRL), because its self-paced design dissociates response inhibition capacity from motivational aspects of behavior (Bizarro et al., 2003; Doughty and Richards, 2002; Hill et al., 2012; Watterson et al., 2015). Here, adult control and *caMek1, Slc32A1:Cre* mice were trained to initiate trials via a nose-poke which resulted in the presentation of sweetened condensed milk in the reward receptacle. Mice were then placed on an FMI schedule, where a time delay between the initiating nose-poke and the availability of reinforcement in the reward receptacle was implemented (Figure 8G). Reward was delivered only if the time between the initiating nose-poke and attempt to obtain reward (inter-response time, or IRT) exceeded a pre-determined withholding period. If mice prematurely accessed the reward receptacle, no reward was delivered.

Following initial training on a FMI with a very short (0.5s) response-withholding period, we measured mouse performance when the withholding period was extended to 2s, 4s, and finally, 8s. We observed a main effect of FMI schedule irrespective of genotype, such that IRTs increased as the FMI withholding period increased ($F(2, 62) = 535.12$, $p < 0.01$). Importantly, mutants showed clear evidence of impaired acquisition of the FMI task. We found a main effect of genotype on the mean median IRT during the first 5 days of each FMI schedule (acquisition period), in which mutant mice had relatively lower IRTs compared to control mice ($F(1, 62) = 18.73$, $p < 0.01$) (Figure 8H). In further support of reduced response inhibition capacity, mutant mice exhibited increased variability in their IRTs as measured by the coefficient of quartile variation (CQV) during acquisition ($F(1, 62) = 31.73$, $p < 0.01$) and asymptotic performance (defined as the last five days of the FMI) ($F(2, 62) = 5.055$, $p < 0.001$) across all schedules (Figure 8I). Median IRTs during the asymptotic phase in mutants and controls were not statistically different in any schedule (Figure 8H inset). Thus, these data suggest that mutant mice are capable of learning to inhibit reinforced responses for up to 4 s but show a significant delay in acquiring this capability.

Due to *Slc32A1:Cre*-mediated recombination within subcortical circuitry, it is possible that altered reward pathway activity influenced FMI performance. The latency to initiate (LTI) a trial provides a measure of motivation; for example, rats administered amphetamine show a reduction in LTI in a related

task (Rojas-Leguizamón et al., 2018). However, we noted that mutants did not differ from controls in the median LTI at 2s and 4s, indicating that motivation to obtain rewards was not significantly altered between conditions (Tukey's b post-hoc test - 2s: $t(21) = 1.39$, $p=0.18$; 4s: $t(21) = -0.29$, $p=0.77$) (Figure 8J). We found that during the 8s FMI, mutant mice exhibited a statistically significant increase in LTI ($t(20) = 2.43$, $p < 0.05$). This apparent loss of motivation is likely due to the fact that the mean median asymptotic IRT did not reach the 8s criterion even after 32 days of testing (control: 8.45s ± 1.04; mutant: 7.26s ± 1.09) and is also consistent with the statistically significant reduction in mean obtained reinforcers at the 8s FMI (Figure 8K). Collectively, our data indicate that altered GABAergic circuitry regulates acquisition of response inhibition capacity in mice and may contribute to ADHD phenotypes associated with the RASopathies.

Discussion

Here, we show that GABAergic neuron-autonomous MEK1 hyperactivation causes the death of a subset of immature GABAergic neurons in the embryonic subpallium and is associated with a selective reduction in PV-CIN density, but not SST-CINs, in adulthood. We observed a significant reduction in perisomatic GABAergic synapses on layer 2/3 PNs and forebrain hyperexcitability, but a surprising increase in the extent of PNN accumulation in mutant PV-CINs. While mutants displayed relatively normal performance in assays of locomotion, sociability, and anxiety, we found notable defects in acquisition of behavioral response inhibition capacity, which has been linked to ADHD. These data suggest that GABAergic neuron-autonomous MEK1 hyperactivation, but not loss of ERK1/2, selectively regulates embryonic PV-CIN survival and is an important contributor to seizure risk and cognitive deficits in the RASopathies.

While expression of ERK/MAPK pathway components is widespread, our findings reinforce the notion that expression levels are variable, and activation of this cascade is highly cell-type dependent. Cell-specific transcriptomic experiments have reported that RNA levels of *Mapk1*/*Erk2* and *Map2k1/Mek1*, but

not *Mapk3/Erk1* or *Map2k2/Mek2*, are lower in CINs relative to PNs (Mardinly et al., 2016). We have extended these findings to show that protein levels of MAPK1/ERK2 and MAP2K1/MEK1 are lower in CINs than in surrounding PNs. Reduced expression of pan-ERK/MAPK components may contribute to the typically low levels of phosphorylated ERK1/2 in CINs. A more stringent degree of ERK/MAPK recruitment is expected to limit activity-dependent transcription in CINs, indeed, the experience-dependent transcriptional response in V1 PV-CINs is significantly smaller relative to PNs (Hrvatin et al., 2018). Further analysis of activity-dependent transcription in CINs of ERK/MAPK-mutant mice may reveal how CIN-specific functional properties are encoded (Tyssowski et al., 2018).

Given the reduced level of ERK/MAPK signaling in CINs, it is perhaps not surprising that loss of ERK1/2 did not significantly alter GABAergic neuron migration or the establishment of CIN number. This contrasts with the significant neuronal death that occurs by P4 in cortical layer 5 when ERK1/2 is deleted in developing excitatory neurons (Xing et al., 2016). These data also indicate that BDNF, GDNF, and NRG1 regulate early GABAergic migration and differentiation via ERK/MAPK independent cascades (Bae et al., 2010; Fazzari et al., 2010; Flames et al., 2004; Perrinjaquet et al., 2011; Pozas and Ibanez, 2005). Notably, the early lethality of *Erk1*$^{-/-}$*, Erk2*$^{fl/fl}$, *Slc32A1:Cre* mutants significantly limited the extent of our analysis, but points to a critical requirement for ERK1/2 in the function or development of an as yet unidentified GABAergic population. The use of a Cre-line with better specificity for developing CINs may help provide a more comprehensive understanding of ERK1/2 function during later, activity-dependent stages of GABAergic circuit development. In addition, the degradation of ERK2 following Cre-mediated gene recombination is likely prolonged relative to ectopic overexpression of caMEK1 under the control of a strong CAG promoter. Thus, at very early stages of GABAergic development it may be difficult to directly compare cellular mechanisms between these two strains.

Defects in GABAergic circuitry have been implicated in pathogenesis of Rett, Fragile X, schizophrenia and many other neurodevelopmental diseases (Chao et al., 2010; Cui et al., 2008; Steullet et al., 2017). Reduced PV-CIN number is often observed, however, the mechanism of loss is poorly understood. In our study, we show that increased MEK1 signaling is sufficient to disrupt the establishment

of CIN number during embryogenesis. We demonstrate that MEK1 hyperactivation drives the GABAergic-neuron autonomous activation of caspase-3 and death of a subset of immature neurons in the embryonic ganglionic eminences. The selective reduction in PV-CIN density in the postnatal cortex suggests these early dying neurons were committed to the PV lineage. The death of this specific subset of GABAergic neurons occurs much earlier than the typical period of programmed cell death for CINs (Denaxa et al., 2018; Southwell et al., 2012) . Notably, *caMek1* expression in cortical excitatory neurons is not associated with significant neuronal loss during development (Nateri et al., 2007; Xing et al., 2016). Though ERK/MAPK typically acts as a promoter of cell survival, apoptotic death by sustained ERK/MAPK activity has been described in certain contexts (Cagnol and Chambard, 2010; Martin and Pognonec, 2010). It will be important to evaluate whether treatment with pharmacological MEK1/2 inhibitors or antioxidants during embryogenesis is capable of sustained restoration of CIN number in *caMek1*, *Slc32A1:Cre* mice. PV-CIN sensitivity to MEK1 hyperactivation may not only be an important factor in RASopathy neuropathology, but could be a relevant mechanism in other conditions that involve indirect activation of ERK/MAPK signaling during embryogenesis, such as schizophrenia, Fragile X Syndrome, or prenatal stress (Fowke et al., 2018).

Recent scRNAseq analyses suggest the mature transcriptional signature of cardinal CIN subtypes is not fully specified until CINs migrate into the cortex (Mayer et al., 2018; Paul et al., 2017; Sandberg et al., 2018). MEF2C, a known substrate of ERK1/2 and p38 signaling, was identified as a transcription factor expressed early in the presumptive PV lineage, the deletion of which also leads to the selective reduction of PV-CINs (Mayer et al., 2018). Consistent with past in situ data, we found that MEF2C immunolabeled cells were present in the cortex and ventro-lateral regions of the E13.5 subpallium in wild-type mice, but not in the proximal regions of the subpallial mantle zone where cleaved caspase-3^{+} GABAergic neurons were observed in mutants (data not shown) (Mattar et al., 2008). Thus, regulation of MEF2C seems unlikely to mediate early GABAergic neuron apoptosis in caMEK1 mutants. While further research is necessary, the selective vulnerability of presumptive PV-CINs to hyperactive MEK1 signaling may not be dependent upon a specific downstream transcriptional target. Compared to transcriptional networks, less is known

regarding the function of many post-translational modifications during CIN specification. Our data hint at selective roles for kinase signaling networks at an early stage of CIN lineage differentiation.

Despite the effect of caMEK1 on early GABAergic neuron survival, the physiological maturation of mature *caMek1*-expressing PV-CINs was not significantly impeded. Surviving PV-CINs retained a characteristic fast-spiking signature with only minor differences in intrinsic electrophysiological parameters. We noted a modest, but statistically significant decrease in perisomatic inhibitory synapse number on cortical PNs in mutant mice. As might be expected, a subset of mutant animals exhibited forebrain hyperexcitability and sudden behavioral arrest similar to that reported in animal models of mild seizures. Overexpression of a similar *caMek1* mutation with *CamKII:Cre* has also been shown to cause seizure-like activity (Nateri et al., 2007). Overall, our findings indicate that MEK1 hyperactivation in GABAergic neurons could increase the risk of epilepsy seen in RASopathies.

The PNN is a critically important structure involved in the maturation of cortical circuitry with an important role in protecting PV-CINs from oxidative stress and limiting synaptic plasticity (Cabungcal et al., 2013; Hensch, 2005a; Hensch, 2005b; Morishita et al., 2015). Mouse models of schizophrenia, Fragile X, and ASDs often exhibit reduced PV-CIN number and typically display a reduction in PNN formation (Steullet et al., 2017). In contrast to these disorders, PNNs appear to respond differently to RASopathy mutations. PV-CINs accumulate extracellular PNNs derived primarily from astrocyte-produced CSPGs (Galtrey and Fawcett, 2007; Sorg et al., 2016). RASopathic astrocytes upregulate secreted ECM-associated CSPGs and promote an increase in the extent of PNN accumulation around PV-CINs (Krencik et al., 2015). Our data is the first to indicate a PV-CIN autonomous role for enhanced PNN accumulation in response to MEK1 hyperactivation. It is thought that increased PNN accumulation on PV-CINs limits the plasticity of cortical regions (Pizzorusso et al., 2002). Modification of PNN levels may serve as a useful therapeutic strategy for the impaired cognitive function and intellectual disability frequently reported in RASopathy individuals (Tidyman and Rauen, 2016).

In addition to intellectual disability, ADHD is frequently diagnosed in Noonan Syndrome and NF1, two common RASopathies (Johnson et al., 2019; Miguel et al., 2015; Pierpont et al., 2015). Abnormal PFC

function has been linked to ADHD (Seidman et al., 2006). Interestingly, we detected significantly reduced P-ERK1/2 levels in PFC PNs of mutant mice, suggesting that RASopathic CINs may alter the global development and function of this brain region. GABAergic signaling is known to be necessary for cortical circuit maturation and MEK1 hyperactivation in CINs appears to be sufficient to disrupt PFC circuit function (Cancedda et al., 2007). We further examined ADHD-related behavioral phenotypes in *caMek1, Slc32A1:Cre* mice by assessing behavioral response inhibition capacity with a fixed-minimum interval (FMI) based task (Rojas-Leguizamón et al., 2018; Watterson et al., 2015). We detected significant deficits in the acquisition of response inhibition dependent behaviors in mutant mice relative to controls. It is plausible that FMI defects in caMEK1 mutants is due to the reduced plasticity of PFC GABAergic circuitry in response to heightened levels of PNN or GABAergic-dependent changes in PN development. Our data show that GABAergic-directed MEK1 hyperactivation is sufficient to drive deficits in behavioral response inhibition possibly associated with ADHD.

Mutations in 'upstream' RASopathy genes modulate a much broader set of downstream cascades when compared to mutations in *Raf* or *Mek1/2*. *Nf1*, *Ptpn11/Shp2*, and *Syngap1* mutations result in a complex constellation of cellular changes, some of which depend upon ERK/MAPK modulation, whereas others involve different signaling cascades (Anastasaki and Gutmann, 2014; Brown et al., 2012). In combination with the findings of (Angara et al., 2019, co-submitted), it is clear that PV-CIN development is particularly sensitive to convergent signaling via NF1 and ERK/MAPK. Additional studies of human samples will be necessary to determine whether defective GABAergic circuits are a component of RASopathy pathogenesis. Collectively, our research suggests that hyperactivation of MEK1 in GABAergic neurons represents an important candidate mechanism for epilepsy and cognitive defects in RASopathic individuals.

Acknowledgements

We would like to thank Johan Martinez, Sam Lusk, Julia Pringle, Anna Kreuger, Sarah Sparks, Katie Riordan, Danielle Gonzalez, Elise Bouchal, and Kimberly Holter for their technical contributions to this work. This research is supported by National Institute of Health grants R00NS076661 and R01NS097537 awarded to JMN, R01NS087031 awarded to TRA, and R01NS031768 to WDS.

Author Contributions

Conceptualization, J.M.N, W.D.S, M.C.H, C.W.D, F.S., T.R.A.; Methodology, J.M.N, W.D.S, M.C.H, C.W.D, F.S., T.R.A., S.M., D.M.T.; Investigation, J.M.N, W.D.S, M.C.H, L.T.H., K.N., G.R.B., S.S., N.R.F., K.P.R., T.A.G., G.L., M.F.O., C.W.D, F.S., T.R.A., S.M., D.M.T.; Writing – Original Draft, M.C.H., J.M.N., C.W.D., T.A.G., F.S., T.R.A., S.M., M.F.O., L.T.H., K.N.; Writing – Review & Editing, M.C.H., J.M.N., G.R.B., S.S., N.R.F., K.P.R., D.M.T. ; Funding Acquisition, J.M.N and W.D.S,; Resources, J.M.N, T.R.A., W.D.S., D.M.T., M.F.O., F.S.; Supervision, J.M.N., W.D.S., D.M.T., T.R.A., F.S.

Declaration of Interest

The authors declare no competing interests.

Figure Titles and Legends

Figure 1. Cortical CINs exhibit low levels of ERK/MAPK expression and activity.

(**A-D**) Representative confocal images of *Slc32A1:Cre, Ai9* sensorimotor cortex. Note the robust expression of RFP in brain regions with high densities of GABAergic neurons. (Scale bar = 100 µm) (**E-M**) Immunolabeling for MEK1 (E-G) and ERK2 (H-J) showed comparatively low expression in inhibitory CINs (yellow outlines) when compared to NEUN^{+}/*Ai9*$^{-}$ excitatory neurons (arrowheads) in layer II (n=3). Relatively lower expression of P-ERK1/2 was also detected in inhibitory CINs when compared to excitatory neurons (n=3). (Scale bar = 10 µm) See also Figure S1.

Figure 2. MEK1 hyperactivation leads to a selective reduction in PV-expressing CINs in the postnatal cortex.

(A-H) *caMek1*, *Slc32A1:Cre*, *Ai9* mutant P3.5 (A-D) and P60 (E-H) primary somatosensory cortices exhibit reduced numbers of *Ai9*-expressing CINs in comparison to *Slc32A1:Cre*, *Ai9* controls (quantification in **I**, n=3, mean ± SEM, * = $p < 0.05$). (Scale bar = 100 µm) **(J-Q)** We quantified the proportion of fluorescently co-labeled PV/RFP or SST/RFP co-expressing CINs in the sensory cortex (J). Confocal micrographs of RFP-expressing CINs at P60 demonstrates that the proportion of PV^{+}/RFP^{+} CINs, but not SST^{+}/RFP^{+} CINs, was significantly decreased in mutants (N-P) in comparison to controls (K-M) (quantification in **Q**: n=3, mean ± SEM, * = $p < 0.05$). (Scale bar = 100 µm) **(R-V)** Mutant PV-CINs (T-U, green arrowheads in T) display increased soma size in comparison to control PV-CINs (R-S) (quantification in **V**, n = 21 control neurons, 42 mutant neurons, mean ± SEM, * = $p < 0.001$). PV^{-}/RFP^{+} CINs displayed no qualitative change in soma size (blue arrowheads). (Scale bar = 25 µm) See also Figure S2.

Figure 3. Loss of Erk1/2 does not alter CIN number.

(A-B) Representative images of P6 coronal brain slices show no gross anatomical defects between *Erk1*$^{-/-}$, *Erk2*$^{fl/fl}$, *Slc32A1:Cre*, *Ai9* mutants and *Erk1*$^{-/-}$, *Erk2*$^{fl/wt}$, *Slc32A1:Cre*, *Ai9* controls. **(C-H)** Reduced ERK2 protein was observed in layer V *Ai9*-expressing CINs in mutant primary somatosensory cortices in

comparison to controls. (Scale bar = 3 μm) **(I-L)** No difference in the density of *Ai9*-expressing CINs was observed between mutants and controls (quantification in **M;** n=3, mean ± SEM, $p > 0.05$). (Scale bar = 100 μm) See also Figure S3.

Figure 4. A subset of immature GABAergic neurons undergo cell death during mid-embryogenesis.

(A) E13.5 coronal section of RFP-labeled CINs in the mantle zones of the *Slc32A1:Cre* subpallium during mid-embryogenesis. **(B-F)** Immunolabeling for cleaved caspase 3 (CC3) showed a significant increase in the number of apoptotic profiles in *caMek1, Slc32A1:Cre* mutants (D-E) as compared to controls (B-C) (quantification in **F**; n=3, mean ± SEM, * = $p < 0.05$). (Scale bar = 100 μm) **(G-Q)** Representative confocal z-stacks of CC3 labeled cells from *caMek1, Slc32A1:Cre* embryos (G-N, Scale bar = 2 μm) and *caMek1, Nkx2.1:Cre* embryos (O-Q) show clear colocalization with RFP and a condensed, pyknotic nuclear morphology. See also Figure S4.

Figure 5. caMek1 Slc32A1:Cre CINs maintain typical fast-spiking properties, but a subset of mice exhibit seizure-like phenotypes.

(A) Representative traces from forebrain-penetrating EEG revealed epochs of synchronous firing in 3 of 6 *caMek1 Slc32A1:Cre*, but not control mice. **(B)** Tail vein PTZ injections revealed a significant reduction in mean dose to seizure onset of PTZ (n = 6, mean ± SEM, * = $p < 0.001$). **(C-F)** *caMek1 Slc32A1:Cre* cortices display aberrant clusters of GFAP-labeled astrocytes (**E,** arrowheads, insets in **F**) that were not observed in controls (C-D) (n=3). (Scale bar = 100 μm) **(G)** Representative current clamp recordings of FS CINs in P21 *Nkx2.1:Cre Ai9* and *caMek1 Nkx2.1:Cre Ai9* mutant cortices. **(H)** Mutant CINs had a significantly reduced FI slope in comparison to controls (mean ± SEM, $p < 0.05$). **(K)** Summary table of FS CIN intrinsic properties. See also Figure S5.

Figure 6. Layer 2/3 excitatory neurons in caMEK1 Slc32A1:Cre mice display reduced perisomatic inhibitory innervation.

(A-F) Representative high-resolution confocal Airyscan images of triple immunolabeled cortical sections for Ai3/EYFP, VGAT, and NEUN. Excitatory neuron perisomatic domains were outlined and quantification of VGAT-labeled pixels revealed that mutants have a significant reduction in the amount of perisomatic VGAT-labeling **(A-F)** (Scale bar = 3 µm), but not neuropil VGAT-labeling **(G-J)** (Scale bar = 10 µm), in comparison to controls (quantification in **K**; perisomatic - n = 48 control, 53 mutant neurons; neuropil - n = 33 control, 30 mutant regions, mean ± SEM, * = $p < 0.05$).

Figure 7. MEK1 hyperactivation drives enhanced PNN accumulation on PV-CINs.

(A-H) P60 representative coronal sections of *Slc32A1:Cre Ai3* (A-C) and *caMek1 Slc32A1:Cre Ai3* (D-F) cortices immunolabeled for GFP, WFA, and PV. The WFA channel was imaged using the same acquisition settings. A significant increase in WFA-labeled area per neuron was detected in mutant cortices as compared to controls (quantification in **G**; n = 63 control, 54 mutant neurons, mean ± SEM, * = $p < 0.001$). Analysis of WFA-labeling intensity also yielded a significant increase in integrated density in mutant CINs (quantification in **H**; n = 63 control, 54 mutant neurons, mean ± SEM, * = $p < 0.001$). (Scale bar = 100 µm) **(I-L)** Expression of the DNA oxidation marker 8-oxo-dg expression in WFA^+ *caMek1 Slc32A1:Cre* CINs (K-L) was qualitatively unchanged when compared to control WFA^+ CINs (I-J). (Scale bar = 25 µm)

Figure 8. caMEK1 Slc32A1:Cre mice exhibit reduced behavioral response inhibition capacity.

(**A-F**). P-ERK1/2 labeling in PFC PNs is significantly reduced in mutants as compared to controls. Note the decrease in RFP^+ CINs in the mutant PFC (E) relative to control (B) (n=3). (Scale bar = 100 µm) **(G)** Schematic of the Fixed-minimum Interval (FMI) task. **(H)** Mutant mice had a significant reduction in mean median IRT during FMI acquisition in 2s and 4s schedules (n=12, mean ± SEM, * = $p < 0.05$). **(I)** Mutant mean CQV of IRTs during both acquisition and asymptotic phases was significantly increased in 2s, 4s, and 8s FMI schedules (mean ± SEM, * = $p < 0.05$). **(J)** Median acquisition and asymptotic LTI was significantly increased in the FMI 8s, but not in the 2s and 4s schedules (mean ± SEM, * = $p < 0.05$).

(K) Mutant mice had a reduction in mean acquisition ORs at 4s and a significant reduction in both mean acquisition and asymptotic ORs during the 8s FMI (mean ± SEM, * = $p < 0.05$).

STAR Methods

Mice

All transgenic mice were handled and housed in accordance with the guidelines of the Institutional Animal Care and Use Committee at Arizona State University, the University of Arizona, and Barrow Neurological Institute. Mice were kept on a daily 12-hour light-dark cycle and were fed *ad libitum*. *Slc32A1:Cre*$^{+/+}$, *Dlx5/6:Cre*$^{+/-}$, or *Nkx2.1:Cre*$^{+/-}$ mice were crossed with *CAG-lox-STOP-lox-Mek1*$^{S217/221E+/-}$ (caMEK1) mice to generate mutants expressing *caMek1* in Cre-expressing cell types. *CaMek1* mice were kindly provided by Dr. Maike Krenz and Dr. Jeffrey Robbins. Loss-of-ERK1/2 mouse mutants were generated with *Erk1/Mapk3*$^{-/-}$ mice possessing a neo-insertion in exons 1-7 and *Erk2/Mapk1*$^{fl/fl}$ mice with a loxp flanked exon 2. Littermates expressing Cre-Recombinase were utilized as controls for most experiments, unless otherwise indicated. Cre-dependent tdTomato (*Ai9*) or eYFP (*Ai3*) strains were used to endogenously label Cre-expressing cells for visualization purposes. Genomic DNA was extracted from tail or toe samples for standard genotyping by PCR using the following primer combinations: (listed 5'-3'): Cre – TTCGCAAGAACCTGATGGAC and CATTGCTGTCACTTGGTCGT to amplify a 266 bp fragment; *Erk1/Mapk3* –AAGGTTAACATCCGGTCCAGCA, AAGCAAGGCTAAGCCGTACC, and CATGCTCCAGACTGCCTTGG to amplify a 571 bp segment wild type and a 250 bp segment KO allele; *Erk2/Mapk1* – AGCCAACAATCCCAAACCTG, and GGCTGCAACCATCTCACAAT amplify 275 bp wild-type and 350 bp floxed alleles; *caMek1*$^{S217/221E}$ -GTACCAGCTCGGCGGAGACCAA and TTGATCACAGCAATGCTAACTTTC amplify a 600 bp fragment; *Ai3/Ai9* – four primers were used - AAGGGAGCTGCAGTGGAGTA, CCGAAAATCTGTGGGAAGTC, ACATGGTCCTGCTGGAGTTC, and GGCATTAAAGCAGCGTATCC amplify a 297 bp wt Rosa26 segment and a 212 bp *Ai3*/*Ai9* allele.

Tissue Preparation and Immunostaining

Mice of the appropriate postnatal age were anesthetized and transcardially perfused with PBS followed by cold 4% PFA in PBS. Brains were dissected, post-fixed at 4°C, and sectioned with a vibratome or cryopreserved with 30% sucrose and sectioned with a cryostat. Free-floating sections were incubated in

primary antibody solution consisting of 1X PBS with 0.05 - 0.2% Triton and 5% Normal Donkey Serum (NDS). Sections were then incubated in species-specific, fluorescently-conjugated secondary antibodies in blocking solution overnight. For embryonic sections, timed-bred embryos were collected at the appropriate embryonic age, immersion fixed in cold 4% PFA in 1X PBS and cryopreserved in serial sucrose concentrations (15%, 25% in 1X PBS) until fully infiltrated. Embryonic brain sections were cryosectioned and directly mounted onto Fisher Superfrost Plus slides. Sections were gently rinsed in 1X PBS 0.05% Triton, incubated in blocking solution (1X PBST 0.05% Triton and 5% NDS) and incubated overnight in primary antibody prepared in blocking solution. The primary antibodies used in these experiments were: goat anti-parvalbumin (Swant, 1:1000), rabbit anti-somatostatin (Peninsula, 1:1000), biotin-conjugated WFA (Vector, 60ug/mL), chicken anti-GFP (Aves, 1:1000), chicken anti-RFP (Rockland, 1:1000), rabbit anti-P-ERK (Cell Signaling, 1:1000), rabbit anti-MEK1 (Abcam, 1:1000), rabbit anti-ERK2 (Abcam, 1:1000), rabbit anti P-ERK1/2 (Cell Signaling, 1:1000), mouse anti-NEUN (Millipore 1:1000), rabbit anti-cleaved caspase 3 (Cell Signaling, 1:1000), rabbit anti-GFAP (Abcam 1:1000), rabbit anti-VGAT (Synaptic Systems, 1:1000), and mouse anti-8-oxo-DG (R&D Systems, 1:1000). Tissue was then washed in 1X PBS 0.05% Triton and incubated in fluorescently conjugated secondary antibody solution before rinsing and cover-slipping for microscopic analysis. Alexa-Fluor 488, 568, and 647 conjugated anti-rabbit, anti-goat, and anti-chicken antibodies were diluted to 1:1000 in 1X PBS 0.05 – 0.2% Triton and 5% NDS. Streptavidin-conjugated fluorophores were used to visualize WFA labeling. Representative images were collected on a Zeiss (LSM710 & LSM800) laser scanning confocal microscope and optimized for brightness and contrast in Adobe Photoshop.

Image Analysis

Images of at least three anatomically matched sections that include a brain region of interest were quantified for labeled cell density by observers blind to genotype. For estimating labeled cell density in the cortex, a column spanning all cortical layers was defined, the cross-sectional area measured, and the number of labeled cells was assessed. The proportion of cells co-labeled with Cre-dependent fluorescent reporters

was also determined for select experiments. Quantification of cellular labeling was averaged across all images collected from an individual mouse. At least three mice were collected for each genotype and results were analyzed using Student's t-tests unless indicated otherwise.

We quantified the extent of inhibitory synapse labeling in the perisomal domain of excitatory neurons from confocal images of VGAT/NeuN/GFP co-labeled sections. Confocal images were collected using optimal Airyscan settings for a 63x 1.4 NA objective on a Zeiss LSM800 with the same acquisition parameters, laser power, gain, and offset for VGAT detection. $NeuN^{+}/GFP^{-}$ neurons in S1 layer 2/3 with a pyramidal morphology and residing 5-10µm from the tissue section surface were randomly selected by a blinded observer. $NeuN^{+}$ soma were outlined in Photoshop and a ring 1.8µm in thickness was then established to specify the perisomatic space. VGAT-immunolabeling from perisomatic regions of interest were imported into ImageJ where a moment-preserving autothreshold algorithm, "Moments", was utilized to define the total area of perisomatic VGAT-labeling in an unbiased manner. Perisomal VGAT-labeled area was then normalized to the total perisomatic area for that neuron. A total of 48 control and 53 mutant neurons from three different mice were analyzed. A similar approach was utilized to quantify VGAT labeling in areas enriched in dendrites by analyzing randomly selected regions of the layer 2/3 neuropil that did not incorporate any NeuN-labeled soma.

EEG Recordings and Seizure Threshold Assessment

Adult *caMek1*, *Slc32A1:Cre* mutant and *Slc32A1:Cre* control mice were assessed for epileptiform activity with bilateral 175µm tungsten wires implanted in the forebrain. After recovery from electrode implantation, mice were connected to suspended EEG leads, housed individually, and monitored daily in home cages for seizure-like activity using a 128 channel Natus Medical EEG machine. EEG recordings were examined for synchronous firing between hemispheres and representative epileptiform traces were acquired. Following intracranial recording, mice were injected with the seizure inducing compound, Pentylenetetrazol (PTZ; Sigma P6500). Mice were gently restrained and the tail vein was intravenously injected with 0.34ml/min of 5mg/mL PTZ in 0.9% saline 10USP heparin by automated pump. Initial onset

of seizure was defined as the first sign of involuntary movement by an observer blinded to genotype. Time to seizure was recorded and PTZ μg/g of body weight was calculated.

Slice electrophysiology

caMek1$^{+/-}$*, Nkx2.1:Cre*$^{+/-}$*, Ai9*$^{+/-}$ mutant and *Nkx2.1:Cre*$^{+/-}$*, Ai9*$^{+/-}$control mice were sacrificed between postnatal day 21 to 24 and used for the in vitro slice electrophysiology. Brain slicing was performed as reported previously (Nichols et al., 2018). In brief, mice were deeply anesthetized by isoflurane inhalation before decapitation. Brains were quickly removed and the coronal slices (350 μM) of the somatosensory cortex were produced on a vibratome (VT 1200; Leica, Nussloch, Germany) in fully oxygenated (95% O_2, 5% CO_2), ice-cold artificial cerebral spinal fluid (aCSF) containing (in mM): 126 NaCl, 26 $NaHCO_3$, 2.5 KCl, 10 glucose, 1.25 $Na_2H_2PO_4 \cdot H_2O$, 1 $MgSO_4 \cdot 7H_2O$, 2 $CaCl_2 \cdot H_2O$, pH 7.4. The slices were incubated in the same aCSF at 32ºC for 30min before being allowed to recover at room temperature for an additional 30 min before patch clamp recordings were started.

After recovery, slices were transferred into recording chamber and perfused continuously with aCSF of 32ºC at a rate of 1-2 ml/min. Then whole-cell patch clamp recordings were performed on tdTomato-positive fast-spiking (FS) interneurons in the somatosensory cortex layer V/VI (L5/6) by using an Axon 700B amplifier. The FS neurons were identified by lack of an emerging apical dendrite and their intrinsic firing response to current injection (Agmon & Connors, 2018; Anderson et al., 2010; McCormick et al., 1985). Clampex 10.6 (Molecular Devices) was used to collect data and pipettes (2-5 MΩ) were pulled from borosilicate glass (BF150-110-10, Sutter Instruments) by using sutter puller (Model P-1000, Sutter Instruments), filled with an internal solution that contains (in mM): 135 K-Gluconate, 4 KCl, 2 NaCl, 10 HEPES, 4 EGTA, 4 Mg ATP and 0.3 Na Tris. The stability of the recordings was monitored during the experiments, and only the recordings with the series resistances (R_s) less than both 25 MΩ and 20% of the membrane resistances were chosen for analysis. For the input resistance calculation, the steady plateau of the voltage responding to the current input of -50 pA step with 1 s duration was used and intrinsic parameters were measured as previously reported (Nichols et al., 2018). Adaptation index was calculated

as the ratio of the 1st interspike interval over the last (i.e. $F_{1st\ ISI}/F_{last\ ISI}$). The frequency (F) – current (I) slope was calculated as the number of induced action potentials (APs) divided by the current step (number of APs at 150pA-number of APs at 100pA)/(150pA-100pA). Unpaired Student's t-test and two-way ANOVA with Bonferroni post hoc tests were used for statistical analysis.

Behavioral Testing

Open Field Testing

The open field test was used to test voluntary locomotor capabilities and anxiety-like behavior. The apparatus consisted of a 40x40cm arena enclosed by 30cm high opaque walls. A single 60W bulb was positioned to brightly illuminate the center of the chamber with dim lighting near the walls. Mice were placed into the apparatus and recorded for a total of 10 minutes. Video data were analyzed for total distance traveled and time spent in the center quadrant.

Elevated Plus Maze

The elevated plus maze was constructed from black polycarbonate, elevated 81cm off the ground, and oriented in a plus formation with two 12x55cm open arms and two 12x55cm closed arms extending from an open 12x12cm center square. Closed arm walls were 40cm high extending from the base of the arm at the center square. The apparatus was lit with a 60W bulb with light concentrated on the center square. At the beginning of the trial, mice were placed in the center square, facing the south open arm, and recorded while freely exploring for 5 minutes.

Social Approach Assay

The social approach apparatus was made of transparent plexiglass and contained three 20x30x30cm chambers (total dimensions 60x30x30cm) connected by open doorways. Prior to experimental social trials, mice were habituated to the apparatus and allowed to freely explore all three chambers for 5 minutes. At the end of the 5 minutes, mice were removed and placed in their home cage. A sex- and age-matched

stimulus mouse was then placed into a small empty cage in chamber 1 of the apparatus. The experimental mouse was reintroduced to the center chamber (chamber 2) of the apparatus and recorded while freely exploring for 10 minutes. The time spent in the chamber with the stimulus mouse (chamber 1) or the empty chamber (chamber 3) was then measured.

Fixed Minimum Interval (FMI)

Twenty-four adult mice (12 *Slc32A1:Cre* mice: 5 males, 7 females; 12 *caMek1*, *Slc32A1:Cre* mice: 6 males, 6 females) were kept on a 12-hour reverse light-dark cycle. Animals had free access to water in their home cages, but access to food was gradually reduced in the week prior to behavioral training, where 1 hr of food access was provided 30 min after the end of each daily training session. Body weights were maintained such that mice lost no more than 15% of starting body weight. Behavioral testing was conducted in eight MED Associates (St. Albans, VT, USA) modular test chambers (240 mm length × 200 mm width × 165 mm height; ENV-307W). Each chamber was enclosed in a sound- and light-attenuating cabinet (ENV-022V) equipped with a fan for ventilation that provided masking noise of approximately 60dB (ENV-025-F28). The back wall and hinged front door of each chamber were made of Plexiglas. The side walls of the chamber were made of aluminum, and the right wall contained the manipulanda and reward receptacle. The floor was composed of thin metal bars. A circular reward receptacle was positioned in the center of the front panel and equipped with a head entry detector (ENV-302HD), a liquid dipper (ENV-302W-S), and a yellow LED (ENV-321W). The reward receptacle was flanked by a nose-poke device including an LED-illuminator (ENV-314M). The chamber was fitted with a house light (ENV-315W) at ceiling level above the back wall (ENV-323AW) and a 4.5kHz tone generator (ENV-323HAM). Experimental programs were arranged via a MED PC interface connected to a PC controlled by MED-PC IV software. All behavioral sessions were 30 min long, including a 3-min warm-up period during which no stimuli were activated.

Reinforcement Training and Autoshaping. Mice were first trained to obtain 0.1 cc of diluted sweetened condensed milk from the liquid dipper (the reinforcer) in the reward receptacle. Following the 3-min warmup period, a reinforcer was made available, followed by consistent reinforcer delivery at variable, pseudo-randomly selected inter-trial intervals (ITIs) for the remainder of the session (mean = 45 s). No stimuli were activated during ITIs. When the dipper was activated and a reinforcer was available, a 2.9-kHz tone, the head-entry LED, and the house light were turned on. The reinforcer remained available until it was obtained by the mouse, which deactivated the 2.9-kHz tone, the LED, and house light. The dipper remains activated for 2.5s after the mouse obtains the reinforcer. Following 5 sessions of reinforcement training, the procedure was modified for 5 autoshaping sessions which, in the last 8s of each ITI, the LED inside of the nose-poke device was turned on. The nose-poke LED was then turned off and reinforcement was delivered as described. If the mouse nose-poked the device during the time when the LED was on, it was turned off and reinforcement was delivered immediately. The autoshaping procedure was then modified for another 5 sessions such that reinforcement delivery was contingent upon a single nose-poke to the nose-poke device when its LED was illuminated and the ITI was reduced to 10s.

Fixed-Minimum Interval Training. Mice were then trained on the fixed-minimum interval (FMI) schedule. After the 3-min warmup period, the houselight was deactivated. A nose-poke (*initiating response*) activated the nose-poke LED and marked the beginning of the inter-response time (IRT). A subsequent head entry into the reward receptacle (*terminating response*) terminated the IRT. Reinforcement was delivered only if the IRT was longer than the criterion time, which was dependent upon the FMI schedule. IRTs shorter than the criterion time terminated without reinforcement, deactivated the nose-poke LED, and another trial could be immediately initiated. IRTs greater than or equal to the criterion time resulted in delivery of reward, deactivation of the nose-poke LED, a 2.5s duration 2.9kHz tone, and subsequent removal of the liquid dipper. Houselights were then activated for a 10s ITI, after which houselight deactivation indicated a new trial could be initiated via nose-poke. The time between the end of the ITI and the nose-poke initiating response was measured and termed the *latency to initiate* (LTI). All mice were initially trained on an FMI schedule with a criterion time of 0.5s

(FMI 0.5s) until stability was achieved. The FMI 0.5s condition was implemented to acclimate mice to the task and is not used to evaluate response inhibition capacity. Performance was considered stable when a non-significant linear regression for mean median IRTs across 5 consecutive sessions was achieved, using a significance criterion of .05. Following stability on the FMI 0.5s schedule, subjects experience FMI 2s, 4s, and 8s. Each subject was trained to stability.

Data Analysis. Four parameters were tracked on a session-by-session basis: median latency-to-initiate trials (LTI), median inter-response time (IRT), the coefficient of quartile variation (CQV) of IRTs (difference between 1st and 3rd quartile divided by their sum), and the number of obtained reinforcers (ORs). The acquisition phase of each parameter was defined as the mean performance during the first five sessions of each schedule, while the asymptote was defined as the mean during the last five sessions. ANOVAs were conducted to assess statistical significance of time and genotype on FMI schedule and Student's *t*-tests were conducted to examine parameter differences based on genotype.

References

Adviento, B., Corbin, I.L., Widjaja, F., Desachy, G., Enrique, N., Rosser, T., Risi, S., Marco, E.J., Hendren, R.L., Bearden, C.E., et al. (2014). Autism traits in the RASopathies. J Med Genet 51, 10-20.

Alessi, D.R., Saito, Y., Campbell, D.G., Cohen, P., Sithanandam, G., Rapp, U., Ashworth, A., Marshall, C.J., and Cowley, S. (1994). Identification of the sites in MAP kinase kinase-1 phosphorylated by p74raf-1. EMBO J 13, 1610-1619.

Anastasaki, C., and Gutmann, D. (2014). Neuronal NF1/RAS regulation of cyclic AMP requires atypical PKC activation. Human Molecular Genetics 23, 6712-6721.

Anderson, T.R., Huguenard, J.R., Prince, D.A. (2010) Differential effects of Na+-K+ ATPase blockade on cortical layer V neurons. J Physiol. 588,4401-14.

Aoidi, R., Houde, N., Landry-Truchon, K., Holter, M., Jacquet, K., Charron, L., Krishnaswami, S., Yu, B., Rauen, K., Bisson, N., et al. (2018). Mek1(Y130C) mice recapitulate aspects of human cardio-facio-cutaneous syndrome. Disease Models & Mechanisms 11.

Bae, M.H., Bissonette, G.B., Mars, W.M., Michalopoulos, G.K., Achim, C.L., Depireux, D.A., and Powell, E.M. (2010). Hepatocyte growth factor (HGF) modulates GABAergic inhibition and seizure susceptibility. Exp Neurol 221, 129-135.

Berryer, M.H., Chattopadhyaya, B., Xing, P., Riebe, I., Bosoi, C., Sanon, N., Antoine-Bertrand, J., Lévesque, M., Avoli, M., Hamdan, F.F., et al. (2016). Decrease of SYNGAP1 in GABAergic cells impairs inhibitory synapse connectivity, synaptic inhibition and cognitive function. Nat Commun 7, 13340.

Bitanihirwe, B.K., and Woo, T.U. (2014). Perineuronal nets and schizophrenia: the importance of neuronal coatings. Neurosci Biobehav Rev 45, 85-99.

Bizarro, L., Murtagh, C., and Stolerman, I. (2003). Differing effects of nicotine, amphetamine and caffeine on performance of a 5-choice serial reaction time task. Journal of Psychopharmacology 17, A31-A31.

722 Brown, J., Diggs-Andrews, K., Gianino, S., and Gutmann, D. (2012). Neurofibromatosis-1 heterozygosity
723 impairs CNS neuronal morphology in a cAMP/PKA/ROCK-dependent manner. Molecular and Cellular
724 Neuroscience 49, 13-22.
725 Bueno, O.F., De Windt, L.J., Tymitz, K.M., Witt, S.A., Kimball, T.R., Klevitsky, R., Hewett, T.E., Jones,
726 S.P., Lefer, D.J., Peng, C.F., et al. (2000). The MEK1-ERK1/2 signaling pathway promotes
727 compensated cardiac hypertrophy in transgenic mice. EMBO J 19, 6341-6350.
728 Cabungcal, J.H., Steullet, P., Morishita, H., Kraftsik, R., Cuenod, M., Hensch, T.K., and Do, K.Q. (2013).
729 Perineuronal nets protect fast-spiking interneurons against oxidative stress. Proc Natl Acad Sci U S A
730 110, 9130-9135.
731 Cagnol, S., and Chambard, J.C. (2010). ERK and cell death: mechanisms of ERK-induced cell death--
732 apoptosis, autophagy and senescence. FEBS J 277, 2-21.
733 Cancedda, L., Fiumelli, H., Chen, K., and Poo, M. (2007). Excitatory GABA action is essential for
734 morphological maturation of cortical neurons in vivo. Journal of Neuroscience 27, 5224-5235.
735 Cancedda, L., Putignano, E., Impey, S., Maffei, L., Ratto, G.M., and Pizzorusso, T. (2003). Patterned vision
736 causes CRE-mediated gene expression in the visual cortex through PKA and ERK. J Neurosci 23, 7012-
737 7020.
738 Chao, H.T., Chen, H., Samaco, R.C., Xue, M., Chahrour, M., Yoo, J., Neul, J.L., Gong, S., Lu, H.C., Heintz,
739 N., et al. (2010). Dysfunction in GABA signalling mediates autism-like stereotypies and Rett syndrome
740 phenotypes. Nature 468, 263-269.
741 Chattopadhyaya, B., Di Cristo, G., Higashiyama, H., Knott, G.W., Kuhlman, S.J., Welker, E., and Huang,
742 Z.J. (2004). Experience and activity-dependent maturation of perisomatic GABAergic innervation in
743 primary visual cortex during a postnatal critical period. J Neurosci 24, 9598-9611.
744 Chattopadhyaya, B., Di Cristo, G., Wu, C.Z., Knott, G., Kuhlman, S., Fu, Y., Palmiter, R.D., and Huang,
745 Z.J. (2007). GAD67-mediated GABA synthesis and signaling regulate inhibitory synaptic innervation
746 in the visual cortex. Neuron 54, 889-903.

747 Clement, J.P., Aceti, M., Creson, T.K., Ozkan, E.D., Shi, Y., Reish, N.J., Almonte, A.G., Miller, B.H.,
748 Wiltgen, B.J., Miller, C.A., et al. (2012). Pathogenic SYNGAP1 mutations impair cognitive
749 development by disrupting maturation of dendritic spine synapses. Cell 151, 709-723.
750 Cowley, S., Paterson, H., Kemp, P., and Marshall, C.J. (1994). Activation of MAP kinase kinase is
751 necessary and sufficient for PC12 differentiation and for transformation of NIH 3T3 cells. Cell 77, 841-
752 852.
753 Cui, Y., Costa, R., Murphy, G., Elgersma, Y., Zhu, Y., Gutmann, D., Parada, L., Mody, I., and Silva, A.
754 (2008). Neurofibromin Regulation of ERK Signaling Modulates GABA Release and Learning. Cell
755 135, 549-560.
756 Denaxa, M., Neves, G., Rabinowitz, A., Kemlo, S., Liodis, P., Burrone, J., and Pachnis, V. (2018).
757 Modulation of Apoptosis Controls Inhibitory Interneuron Number in the Cortex. Cell Rep 22, 1710-
758 1721.
759 Digilio, M.C., Lepri, F., Baban, A., Dentici, M.L., Versacci, P., Capolino, R., Ferese, R., De Luca, A.,
760 Tartaglia, M., Marino, B., et al. (2011). RASopathies: Clinical Diagnosis in the First Year of Life. Mol
761 Syndromol 1, 282-289.
762 Doughty, A.H., and Richards, J.B. (2002). Effects of reinforcer magnitude on responding under differential-
763 reinforcement-of-low-rate schedules of rats and pigeons. J Exp Anal Behav 78, 17-30.
764 Ehrman, L., Nardini, D., Ehrman, S., Rizvi, T., Gulick, J., Krenz, M., Dasgupta, B., Robbins, J., Ratner, N.,
765 Nakafuku, M., et al. (2014). The Protein Tyrosine Phosphatase Shp2 Is Required for the Generation of
766 Oligodendrocyte Progenitor Cells and Myelination in the Mouse Telencephalon. Journal of
767 Neuroscience 34, 3767-3778.
768 El Idrissi, A., Ding, X.H., Scalia, J., Trenkner, E., Brown, W.T., and Dobkin, C. (2005). Decreased
769 GABA(A) receptor expression in the seizure-prone fragile X mouse. Neurosci Lett 377, 141-146.
770 Fazzari, P., Paternain, A.V., Valiente, M., Pla, R., Luján, R., Lloyd, K., Lerma, J., Marín, O., and Rico, B.
771 (2010). Control of cortical GABA circuitry development by Nrg1 and ErbB4 signalling. Nature 464,
772 1376-1380.

773 Fino, E., Packer, A.M., and Yuste, R. (2013). The logic of inhibitory connectivity in the neocortex.
774 Neuroscientist 19, 228-237.
775 Flames, N., Long, J., Garratt, A., Fischer, T., Gassmann, M., Birchmeier, C., Lai, C., Rubenstein, J., and
776 Marin, O. (2004). Short- and long-range attraction of cortical GABAergic interneurons by Neuregulin-
777 1. Neuron 44, 251-261.
778 Fowke, T.M., Galinsky, R., Davidson, J.O., Wassink, G., Karunasinghe, R.N., Prasad, J.D., Bennet, L.,
779 Gunn, A.J., and Dean, J.M. (2018). Loss of interneurons and disruption of perineuronal nets in the
780 cerebral cortex following hypoxia-ischaemia in near-term fetal sheep. Sci Rep 8, 17686.
781 Gabay, Y., Shahbari-Khateb, E., and Mendelsohn, A. (2018). Feedback Timing Modulates Probabilistic
782 Learning in Adults with ADHD. Sci Rep 8, 15524.
783 Galtrey, C.M., and Fawcett, J.W. (2007). The role of chondroitin sulfate proteoglycans in regeneration and
784 plasticity in the central nervous system. Brain Res Rev 54, 1-18.
785 Garg, S., Lehtonen, A., Huson, S.M., Emsley, R., Trump, D., Evans, D.G., and Green, J. (2013). Autism
786 and other psychiatric comorbidity in neurofibromatosis type 1: evidence from a population-based study.
787 Dev Med Child Neurol 55, 139-145.
788 Gauthier, A., Furstoss, O., Araki, T., Chan, R., Neel, B., Kaplan, D., and Miller, F. (2007). Control of CNS
789 cell-fate decisions by SHP-2 and its dysregulation in Noonan syndrome. Neuron 54, 245-262.
790 Gelman, D., Martini, F., Nobrega-Pereira, S., Pierani, A., Kessaris, N., and Marin, O. (2009). The
791 Embryonic Preoptic Area Is a Novel Source of Cortical GABAergic Interneurons. Journal of
792 Neuroscience 29, 9380-9389.
793 Gelman, D.M., and Marín, O. (2010). Generation of interneuron diversity in the mouse cerebral cortex. Eur
794 J Neurosci 31, 2136-2141.
795 Goldberg, E., Jeong, H., Kruglikov, I., Tremblay, R., Lazarenko, R., and Rudy, B. (2011). Rapid
796 Developmental Maturation of Neocortical FS Cell Intrinsic Excitability. Cerebral Cortex 21, 666-682.

Green, T., Naylor, P.E., and Davies, W. (2017). Attention deficit hyperactivity disorder (ADHD) in phenotypically similar neurogenetic conditions: Turner syndrome and the RASopathies. J Neurodev Disord 9, 25.

Hensch, T. (2005a). Critical period mechanisms in developing visual cortex. Current Topics in Developmental Biology, Vol 69 69, 215-+.

Hensch, T.K. (2005b). Critical period plasticity in local cortical circuits. Nat Rev Neurosci 6, 877-888.

Hill, J.C., Herbst, K., and Sanabria, F. (2012). Characterizing operant hyperactivity in the Spontaneously Hypertensive Rat. Behav Brain Funct 8, 5.

Holter, M.C., Hewitt, L.T., Koebele, S.V., Judd, J.M., Xing, L., Bimonte-Nelson, H.A., Conrad, C.D., Araki, T., Neel, B.G., Snider, W.D., et al. (2019). The Noonan Syndrome-linked Raf1L613V mutation drives increased glial number in the mouse cortex and enhanced learning. PLoS Genet 15, e1008108.

Hrvatin, S., Hochbaum, D.R., Nagy, M.A., Cicconet, M., Robertson, K., Cheadle, L., Zilionis, R., Ratner, A., Borges-Monroy, R., Klein, A.M., et al. (2018). Single-cell analysis of experience-dependent transcriptomic states in the mouse visual cortex. Nat Neurosci 21, 120-129.

Ishii, A., Furusho, M., and Bansal, R. (2013). Sustained Activation of ERK1/2 MAPK in Oligodendrocytes and Schwann Cells Enhances Myelin Growth and Stimulates Oligodendrocyte Progenitor Expansion. Journal of Neuroscience 33, 175-186.

Johnson, E.M., Ishak, A.D., Naylor, P.E., Stevenson, D.A., Reiss, A.L., and Green, T. (2019). PTPN11 Gain-of-Function Mutations Affect the Developing Human Brain, Memory, and Attention. Cereb Cortex 29, 2915-2923.

Kelsom, C., and Lu, W. (2013). Development and specification of GABAergic cortical interneurons. Cell Biosci 3, 19.

Kessaris, N., Magno, L., Rubin, A.N., and Oliveira, M.G. (2014). Genetic programs controlling cortical interneuron fate. Curr Opin Neurobiol 26, 79-87.

Klesse, L.J., Meyers, K.A., Marshall, C.J., and Parada, L.F. (1999). Nerve growth factor induces survival and differentiation through two distinct signaling cascades in PC12 cells. Oncogene 18, 2055-2068.

Krencik, R., Hokanson, K.C., Narayan, A.R., Dvornik, J., Rooney, G.E., Rauen, K.A., Weiss, L.A., Rowitch, D.H., and Ullian, E.M. (2015). Dysregulation of astrocyte extracellular signaling in Costello syndrome. Sci Transl Med 7, 286ra266.

Krens, S.F., Spaink, H.P., and Snaar-Jagalska, B.E. (2006). Functions of the MAPK family in vertebrate-development. FEBS Lett 580, 4984-4990.

Krenz, M., Gulick, J., Osinska, H.E., Colbert, M.C., Molkentin, J.D., and Robbins, J. (2008). Role of ERK1/2 signaling in congenital valve malformations in Noonan syndrome. Proc Natl Acad Sci U S A 105, 18930-18935.

Krishnan, K., Wang, B.S., Lu, J., Wang, L., Maffei, A., Cang, J., and Huang, Z.J. (2015). MeCP2 regulates the timing of critical period plasticity that shapes functional connectivity in primary visual cortex. Proc Natl Acad Sci U S A 112, E4782-4791.

Krueger, D.D., Osterweil, E.K., Chen, S.P., Tye, L.D., and Bear, M.F. (2011). Cognitive dysfunction and prefrontal synaptic abnormalities in a mouse model of fragile X syndrome. Proc Natl Acad Sci U S A 108, 2587-2592.

Kumar, R.A., KaraMohamed, S., Sudi, J., Conrad, D.F., Brune, C., Badner, J.A., Gilliam, T.C., Nowak, N.J., Cook, E.H., Dobyns, W.B., et al. (2008). Recurrent 16p11.2 microdeletions in autism. Hum Mol Genet 17, 628-638.

Lajiness, J.D., Snider, P., Wang, J., Feng, G.S., Krenz, M., and Conway, S.J. (2014). SHP-2 deletion in postmigratory neural crest cells results in impaired cardiac sympathetic innervation. Proc Natl Acad Sci U S A 111, E1374-1382.

Lavdas, A.A., Grigoriou, M., Pachnis, V., and Parnavelas, J.G. (1999). The medial ganglionic eminence gives rise to a population of early neurons in the developing cerebral cortex. J Neurosci 19, 7881-7888.

Li, X., Newbern, J., Wu, Y., Morgan-Smith, M., Zhong, J., Charron, J., and Snider, W. (2012). MEK Is a Key Regulator of Gliogenesis in the Developing Brain. Neuron 75, 1035-1050.

Lim, L., Mi, D., Llorca, A., and Marín, O. (2018). Development and Functional Diversification of Cortical Interneurons. Neuron 100, 294-313.

Madisen, L., Zwingman, T.A., Sunkin, S.M., Oh, S.W., Zariwala, H.A., Gu, H., Ng, L.L., Palmiter, R.D., Hawrylycz, M.J., Jones, A.R., et al. (2010). A robust and high-throughput Cre reporting and characterization system for the whole mouse brain. Nat Neurosci 13, 133-140.

Mardinly, A.R., Spiegel, I., Patrizi, A., Centofante, E., Bazinet, J.E., Tzeng, C.P., Mandel-Brehm, C., Harmin, D.A., Adesnik, H., Fagiolini, M., et al. (2016). Sensory experience regulates cortical inhibition by inducing IGF1 in VIP neurons. Nature 531, 371-375.

Marin, O., and Rubenstein, J. (2001). A long, remarkable journey: Tangential migration in the telencephalon. Nature Reviews Neuroscience 2, 780-790.

Marin, O., and Rubenstein, J. (2003). Cell migration in the forebrain. Annual Review of Neuroscience 26, 441-483.

Martin, P., and Pognonec, P. (2010). ERK and cell death: cadmium toxicity, sustained ERK activation and cell death. FEBS J 277, 39-46.

Mattar, P., Langevin, L.M., Markham, K., Klenin, N., Shivji, S., Zinyk, D., and Schuurmans, C. (2008). Basic helix-loop-helix transcription factors cooperate to specify a cortical projection neuron identity. Mol Cell Biol 28, 1456-1469.

Mayer, C., Hafemeister, C., Bandler, R.C., Machold, R., Batista Brito, R., Jaglin, X., Allaway, K., Butler, A., Fishell, G., and Satija, R. (2018). Developmental diversification of cortical inhibitory interneurons. Nature 555, 457-462.

McCormick, D.A., Connors, B.W., Lighthall, J.W., Prince, D.A. (1985) Comparative electrophysiology of pyramidal and sparsely spiny stellate neurons of the neocortex. J Neurophysiol. 54:782-806.

Mi, D., Li, Z., Lim, L., Li, M., Moissidis, M., Yang, Y., Gao, T., Hu, T.X., Pratt, T., Price, D.J., et al. (2018). Early emergence of cortical interneuron diversity in the mouse embryo. Science 360, 81-85.

Miguel, C.S., Chaim-Avancini, T.M., Silva, M.A., and Louzã, M.R. (2015). Neurofibromatosis type 1 and attention deficit hyperactivity disorder: a case study and literature review. Neuropsychiatr Dis Treat 11, 815-821.

874 Monory, K., Massa, F., Egertová, M., Eder, M., Blaudzun, H., Westenbroek, R., Kelsch, W., Jacob, W.,
875 Marsch, R., Ekker, M., et al. (2006). The endocannabinoid system controls key epileptogenic circuits
876 in the hippocampus. Neuron 51, 455-466.
877 Morishita, H., Cabungcal, J., Chen, Y., Do, K., and Hensch, T. (2015). Prolonged Period of Cortical
878 Plasticity upon Redox Dysregulation in Fast-Spiking Interneurons. Biological Psychiatry 78, 396-402.
879 Nateri, A.S., Raivich, G., Gebhardt, C., Da Costa, C., Naumann, H., Vreugdenhil, M., Makwana, M.,
880 Brandner, S., Adams, R.H., Jefferys, J.G., et al. (2007). ERK activation causes epilepsy by stimulating
881 NMDA receptor activity. EMBO J 26, 4891-4901.
882 Nichols, J., Bjorklund, G.R., Newbern, J., and Anderson, T. (2018). Parvalbumin fast-spiking interneurons
883 are selectively altered by paediatric traumatic brain injury. J Physiol 596, 1277-1293.
884 Okaty, B., Miller, M., Sugino, K., Hempel, C., and Nelson, S. (2009). Transcriptional and
885 Electrophysiological Maturation of Neocortical Fast-Spiking GABAergic Interneurons. Journal of
886 Neuroscience 29, 7040-7052.
887 Ozkan, E.D., Creson, T.K., Kramár, E.A., Rojas, C., Seese, R.R., Babyan, A.H., Shi, Y., Lucero, R., Xu,
888 X., Noebels, J.L., et al. (2014). Reduced cognition in Syngap1 mutants is caused by isolated damage
889 within developing forebrain excitatory neurons. Neuron 82, 1317-1333.
890 Paluszkiewicz, S.M., Martin, B.S., and Huntsman, M.M. (2011). Fragile X syndrome: the GABAergic
891 system and circuit dysfunction. Dev Neurosci 33, 349-364.
892 Parnavelas, J.G. (2000). The origin and migration of cortical neurones: new vistas. Trends Neurosci 23,
893 126-131.
894 Paul, A., Crow, M., Raudales, R., He, M., Gillis, J., and Huang, Z.J. (2017). Transcriptional Architecture
895 of Synaptic Communication Delineates GABAergic Neuron Identity. Cell 171, 522-539.e520.
896 Perrinjaquet, M., Sjostrand, D., Moliner, A., Zechel, S., Lamballe, F., Maina, F., and Ibanez, C. (2011).
897 MET signaling in GABAergic neuronal precursors of the medial ganglionic eminence restricts GDNF
898 activity in cells that express GFR alpha 1 and a new transmembrane receptor partner. Journal of Cell
899 Science 124, 2797-2805.

Pham, T.A., Graham, S.J., Suzuki, S., Barco, A., Kandel, E.R., Gordon, B., and Lickey, M.E. (2004). A semi-persistent adult ocular dominance plasticity in visual cortex is stabilized by activated CREB. Learn Mem 11, 738-747.

Pierpont, E., Hudock, R., Foy, A., Semrud-Clikeman, M., Pierpont, M., Berry, S., Shanley, R., Rubin, N., Sommer, K., and Moertel, C. (2018). Social skills in children with RASopathies: a comparison of Noonan syndrome and neurofibromatosis type 1. Journal of Neurodevelopmental Disorders 10.

Pierpont, E., Tworog-Dube, E., and Roberts, A. (2015). Attention skills and executive functioning in children with Noonan syndrome and their unaffected siblings. Developmental Medicine and Child Neurology 57, 385-392.

Pizzorusso, T., Medini, P., Berardi, N., Chierzi, S., Fawcett, J.W., and Maffei, L. (2002). Reactivation of ocular dominance plasticity in the adult visual cortex. Science 298, 1248-1251.

Pozas, E., and Ibanez, C. (2005). GDNF and GFR alpha 1 promote differentiation and tangential migration of cortical GABAergic neurons. Neuron 45, 701-713.

Pucilowska, J., Puzerey, P., Karlo, J., Galan, R., and Landreth, G. (2012). Disrupted ERK Signaling during Cortical Development Leads to Abnormal Progenitor Proliferation, Neuronal and Network Excitability and Behavior, Modeling Human Neuro-Cardio-Facial-Cutaneous and Related Syndromes. Journal of Neuroscience 32, 8663-8677.

Pucilowska, J., Vithayathil, J., Pagani, M., Kelly, C., Karlo, J.C., Robol, C., Morella, I., Gozzi, A., Brambilla, R., and Landreth, G.E. (2018). Pharmacological Inhibition of ERK Signaling Rescues Pathophysiology and Behavioral Phenotype Associated with 16p11.2 Chromosomal Deletion in Mice. J Neurosci 38, 6640-6652.

Pucilowska, J., Vithayathil, J., Tavares, E., Kelly, C., Karlo, J., and Landreth, G. (2015). The 16p11.2 Deletion Mouse Model of Autism Exhibits Altered Cortical Progenitor Proliferation and Brain Cytoarchitecture Linked to the ERK MAPK Pathway. Journal of Neuroscience 35, 3190-3200.

Rauen, K., Chakravarti, A., and Green, E. (2013). The RASopathies. Annual Review of Genomics and Human Genetics, Vol 14 14, 355-369.

926 Rojas-Leguizamón, M., Baroja, J.L., Sanabria, F., and Orduña, V. (2018). Response-inhibition capacity in
927 spontaneously hypertensive and Wistar rats: acquisition of fixed minimum interval performance and
928 responsiveness to D-amphetamine. Behav Pharmacol 29, 668-675.
929 Rosato-Siri, M., Zambello, E., Mutinelli, C., Garbati, N., Benedetti, R., Aldegheri, L., Graziani, F.,
930 Virginio, C., Alvaro, G., and Large, C. (2015). A Novel Modulator of Kv3 Potassium Channels
931 Regulates the Firing of Parvalbumin-Positive Cortical Interneurons. Journal of Pharmacology and
932 Experimental Therapeutics 354, 251-260.
933 Rudy, B., Fishell, G., Lee, S., and Hjerling-Leffler, J. (2011). Three groups of interneurons account for
934 nearly 100% of neocortical GABAergic neurons. Dev Neurobiol 71, 45-61.
935 Rudy, B., and McBain, C. (2001). Kv3 channels: voltage-gated K+ channels designed for high-frequency
936 repetitive firing. Trends in Neurosciences 24, 517-526.
937 Samuels, I., Saitta, S., and Landreth, G. (2009). MAP'ing CNS Development and Cognition: An ERKsome
938 Process. Neuron 61, 160-167.
939 Sandberg, M., Taher, L., Hu, J., Black, B.L., Nord, A.S., and Rubenstein, J.L.R. (2018). Genomic analysis
940 of transcriptional networks directing progression of cell states during MGE development. Neural Dev
941 13, 21.
942 Seidman, L.J., Valera, E.M., Makris, N., Monuteaux, M.C., Boriel, D.L., Kelkar, K., Kennedy, D.N.,
943 Caviness, V.S., Bush, G., Aleardi, M., et al. (2006). Dorsolateral prefrontal and anterior cingulate cortex
944 volumetric abnormalities in adults with attention-deficit/hyperactivity disorder identified by magnetic
945 resonance imaging. Biol Psychiatry 60, 1071-1080.
946 Selby, L., Zhang, C., and Sun, Q.Q. (2007). Major defects in neocortical GABAergic inhibitory circuits in
947 mice lacking the fragile X mental retardation protein. Neurosci Lett 412, 227-232.
948 Sorg, B.A., Berretta, S., Blacktop, J.M., Fawcett, J.W., Kitagawa, H., Kwok, J.C., and Miquel, M. (2016).
949 Casting a Wide Net: Role of Perineuronal Nets in Neural Plasticity. J Neurosci 36, 11459-11468.

Southwell, D., Paredes, M., Galvao, R., Jones, D., Froemke, R., Sebe, J., Alfaro-Cervello, C., Tang, Y., Garcia-Verdugo, J., Rubenstein, J., et al. (2012). Intrinsically determined cell death of developing cortical interneurons. Nature 491, 109-U172.

Stanco, A., Pla, R., Vogt, D., Chen, Y., Mandal, S., Walker, J., Hunt, R., Lindtner, S., Erdman, C., Pieper, A., et al. (2014). NPAS1 Represses the Generation of Specific Subtypes of Cortical Interneurons. Neuron 84, 940-953.

Steullet, P., Cabungcal, J.H., Coyle, J., Didriksen, M., Gill, K., Grace, A.A., Hensch, T.K., LaMantia, A.S., Lindemann, L., Maynard, T.M., et al. (2017). Oxidative stress-driven parvalbumin interneuron impairment as a common mechanism in models of schizophrenia. Mol Psychiatry 22, 936-943.

Steward, O., Torre, E., Tomasulo, R., and Lothman, E. (1992). Seizures and the Regulation of Astroglial Gene Expression. Epilepsy Research, 197-209.

Stringer, J. (1996). Repeated seizures increase GFAP and vimentin in the hippocampus. Brain Research 717, 147-153.

Suzuki, S., al-Noori, S., Butt, S.A., and Pham, T.A. (2004). Regulation of the CREB signaling cascade in the visual cortex by visual experience and neuronal activity. J Comp Neurol 479, 70-83.

Tamamaki, N., Fujimori, K.E., and Takauji, R. (1997). Origin and route of tangentially migrating neurons in the developing neocortical intermediate zone. J Neurosci 17, 8313-8323.

Tidyman, W., and Rauen, K. (2016). Pathogenetics of the RASopathies. Human Molecular Genetics 25, R123-R132.

Tyssowski, K.M., DeStefino, N.R., Cho, J.H., Dunn, C.J., Poston, R.G., Carty, C.E., Jones, R.D., Chang, S.M., Romeo, P., Wurzelmann, M.K., et al. (2018). Different Neuronal Activity Patterns Induce Different Gene Expression Programs. Neuron 98, 530-546.e511.

Ure, K., Lu, H., Wang, W., Ito-Ishida, A., Wu, Z., He, L.J., Sztainberg, Y., Chen, W., Tang, J., and Zoghbi, H.Y. (2016). Restoration of Mecp2 expression in GABAergic neurons is sufficient to rescue multiple disease features in a mouse model of Rett syndrome. Elife 5.

975 Vong, L., Ye, C., Yang, Z., Choi, B., Chua, S., and Lowell, B.B. (2011). Leptin action on GABAergic
976 neurons prevents obesity and reduces inhibitory tone to POMC neurons. Neuron 71, 142-154.
977 Vorstman, J.A., Staal, W.G., van Daalen, E., van Engeland, H., Hochstenbach, P.F., and Franke, L. (2006).
978 Identification of novel autism candidate regions through analysis of reported cytogenetic abnormalities
979 associated with autism. Mol Psychiatry 11, 1, 18-28.
980 Walsh, K.S., Vélez, J.I., Kardel, P.G., Imas, D.M., Muenke, M., Packer, R.J., Castellanos, F.X., and Acosta,
981 M.T. (2013). Symptomatology of autism spectrum disorder in a population with neurofibromatosis type
982 1. Dev Med Child Neurol 55, 131-138.
983 Watterson, E., Mazur, G.J., and Sanabria, F. (2015). Validation of a method to assess ADHD-related
984 impulsivity in animal models. J Neurosci Methods 252, 36-47.
985 Wichterle, H., Garcia-Verdugo, J.M., Herrera, D.G., and Alvarez-Buylla, A. (1999). Young neurons from
986 medial ganglionic eminence disperse in adult and embryonic brain. Nat Neurosci 2, 461-466.
987 Wichterle, H., Turnbull, D., Nery, S., Fishell, G., and Alvarez-Buylla, A. (2001). In utero fate mapping
988 reveals distinct migratory pathways and fates of neurons born in the mammalian basal forebrain.
989 Development 128, 3759-3771.
990 Wonders, C., and Anderson, S. (2006). The origin and specification of cortical interneurons. Nature
991 Reviews Neuroscience 7, 687-696.
992 Xing, L., Larsen, R., Bjorklund, G., Li, X., Wu, Y., Philpot, B., Snider, W., and Newbern, J. (2016). Layer
993 specific and general requirements for ERK/MAPK signaling in the developing neocortex. Elife 5.
994 Yoon, G., Rosenberg, J., Blaser, S., and Rauen, K. (2007). Neurological complications of cardio-facio-
995 cutaneous syndrome. Developmental Medicine and Child Neurology 49, 894-899.
996 Zhang, Z.W., Zak, J.D., and Liu, H. (2010). MeCP2 is required for normal development of GABAergic
997 circuits in the thalamus. J Neurophysiol 103, 2470-2481.

Figure 1

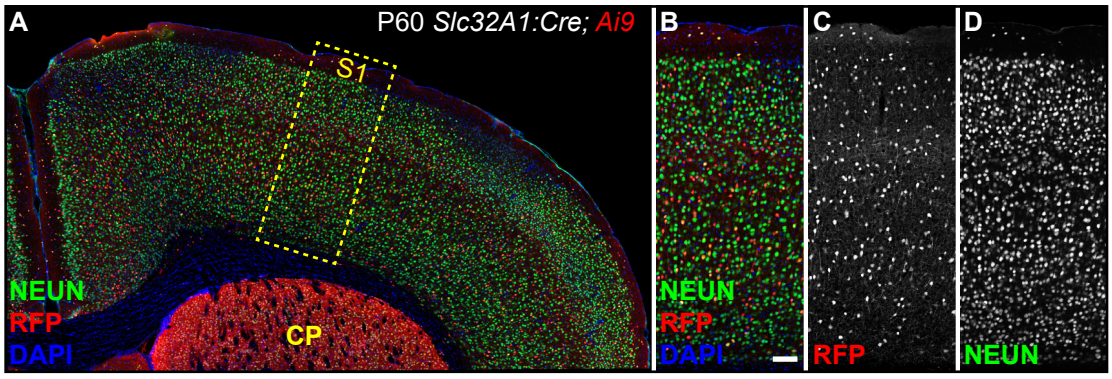

Slc32A1:Cre; Ai9 S1 Layer II/III

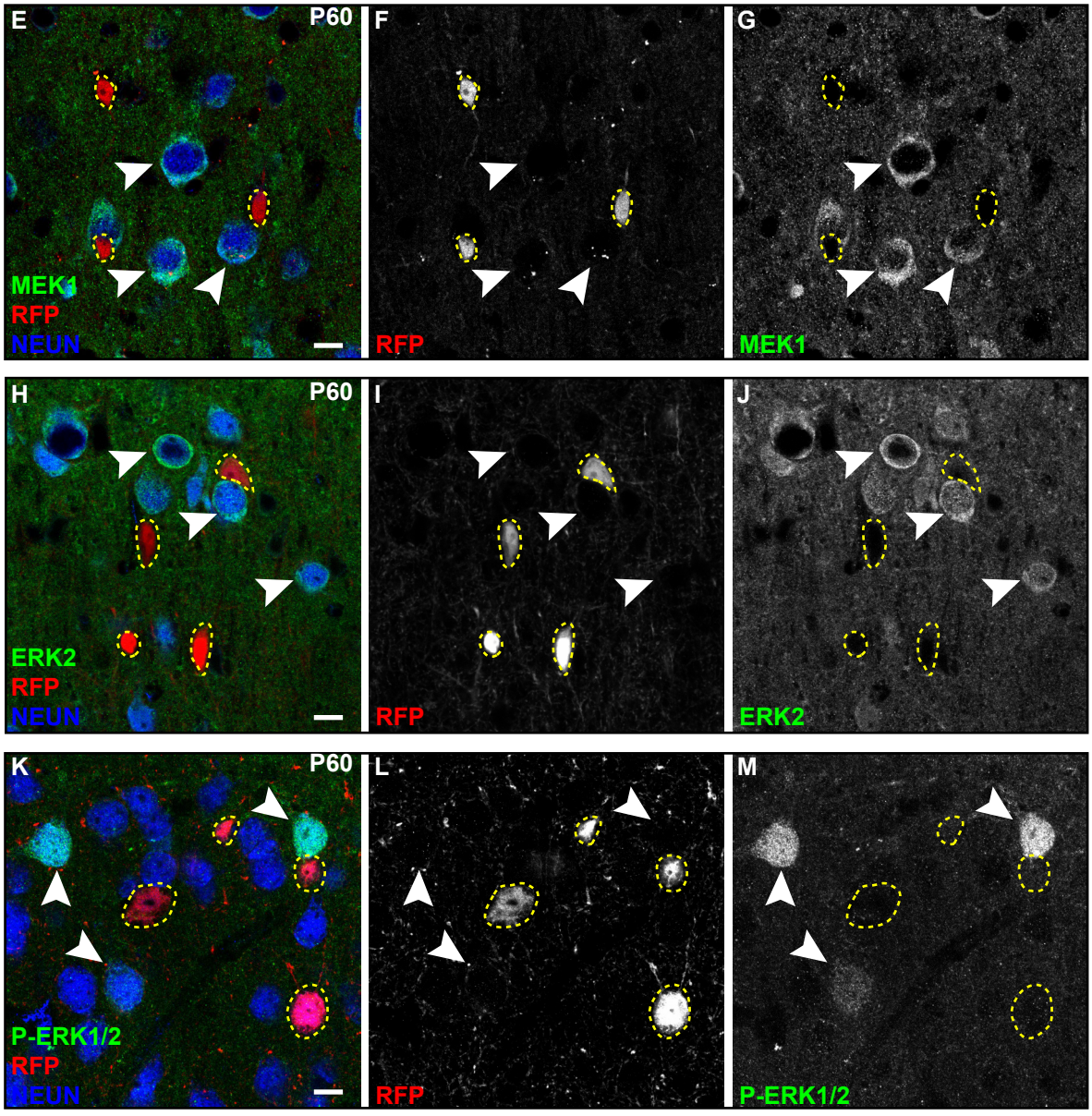

Figure 2

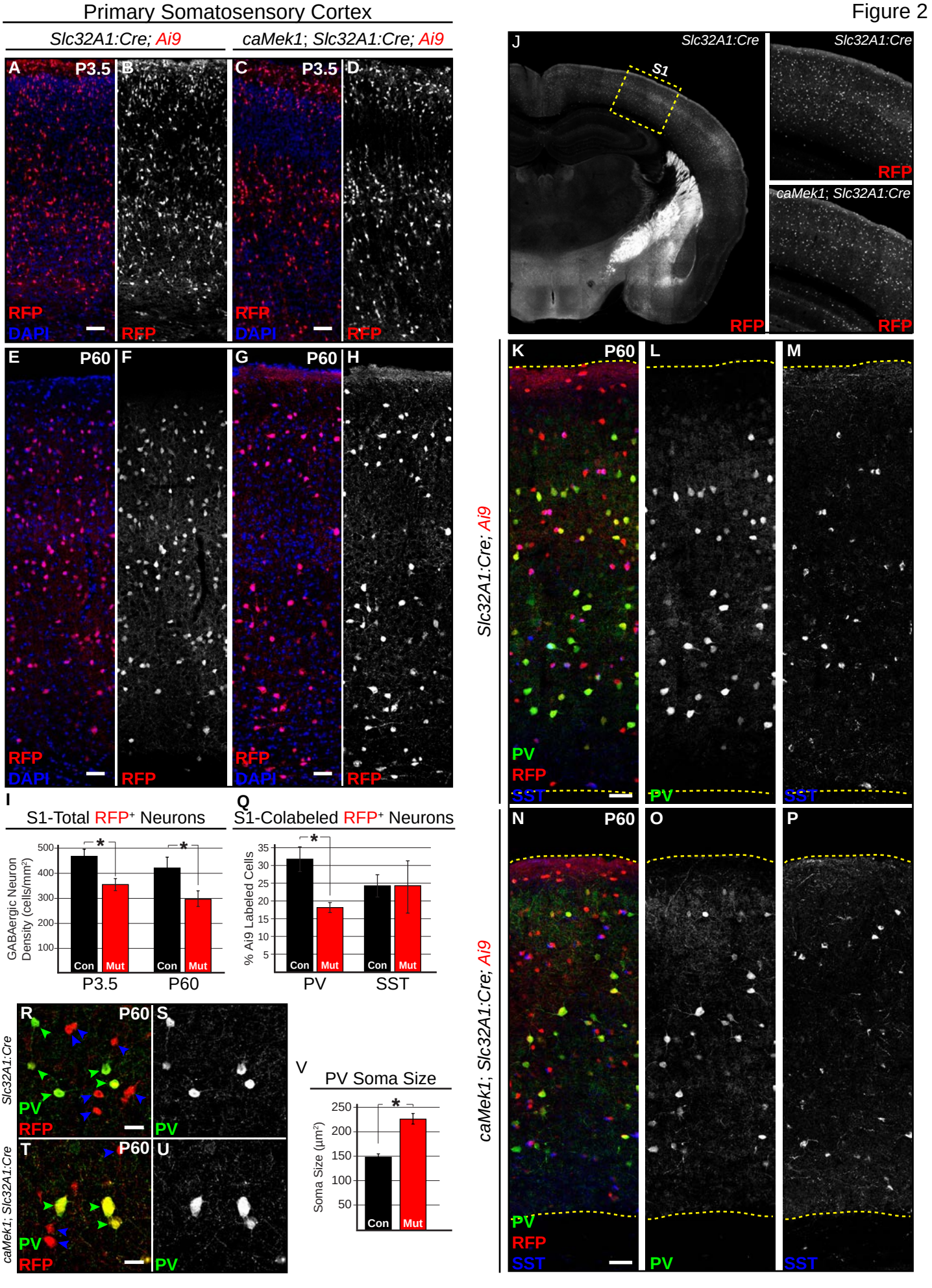

Figure 3

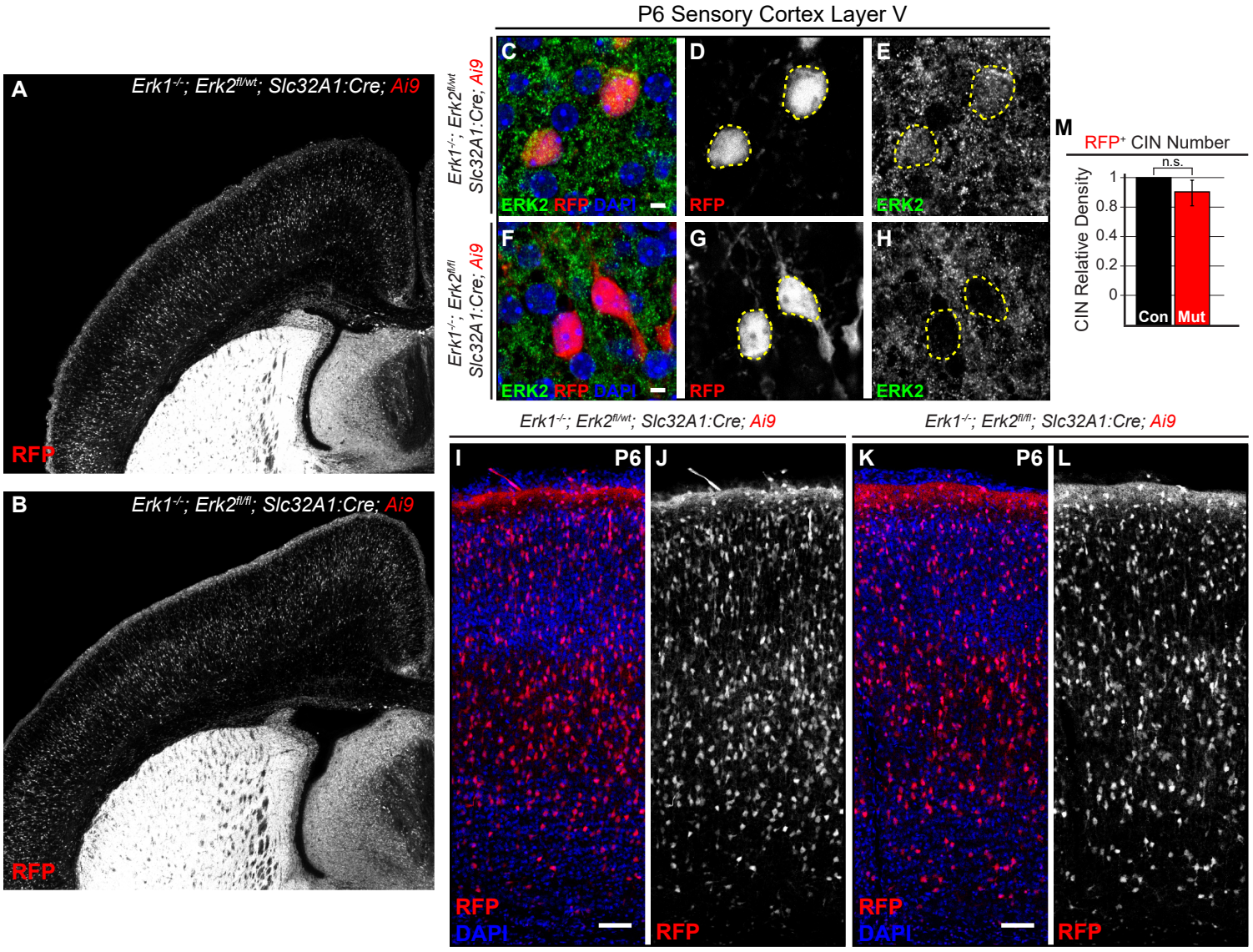

Figure 4

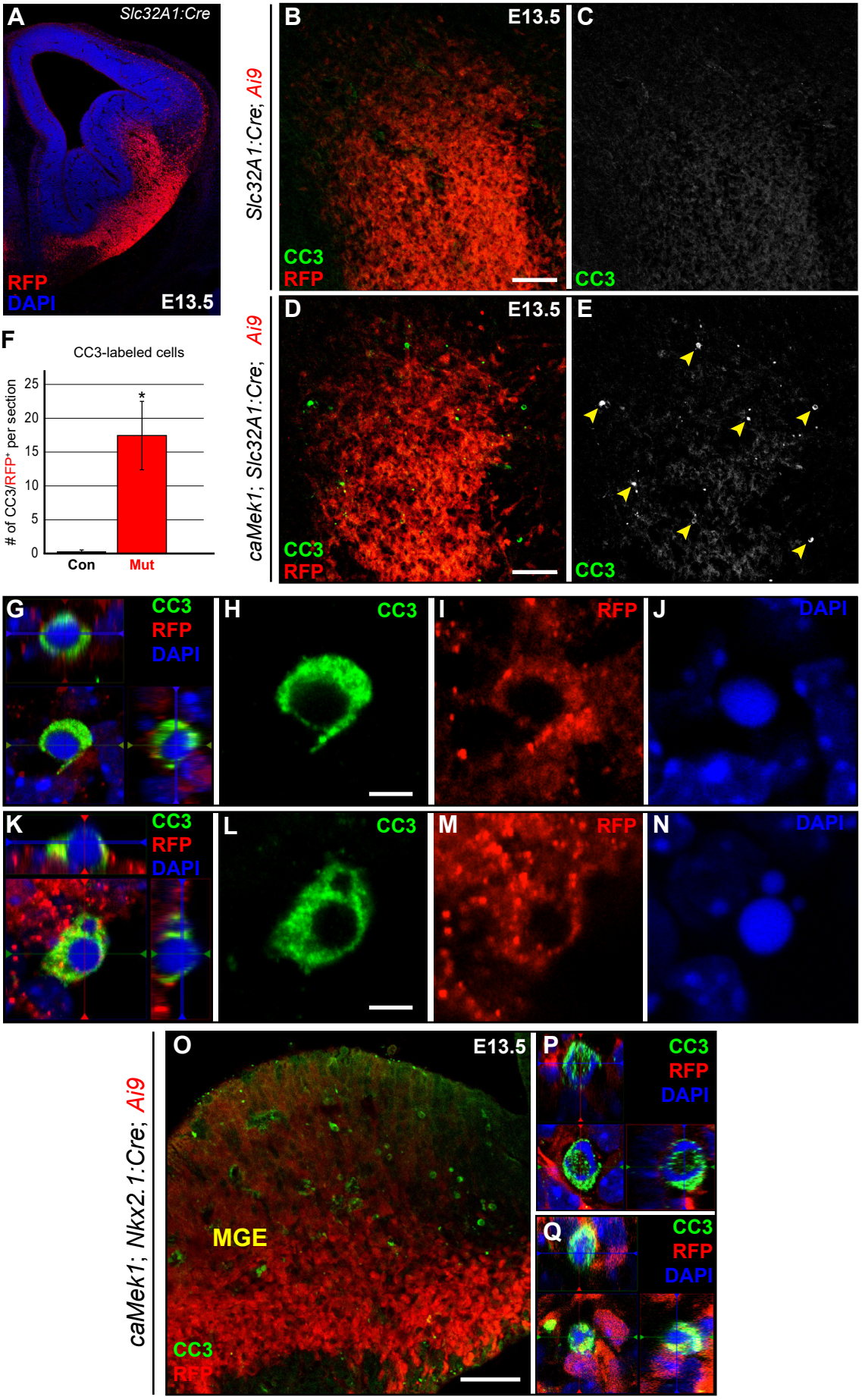

Figure 5

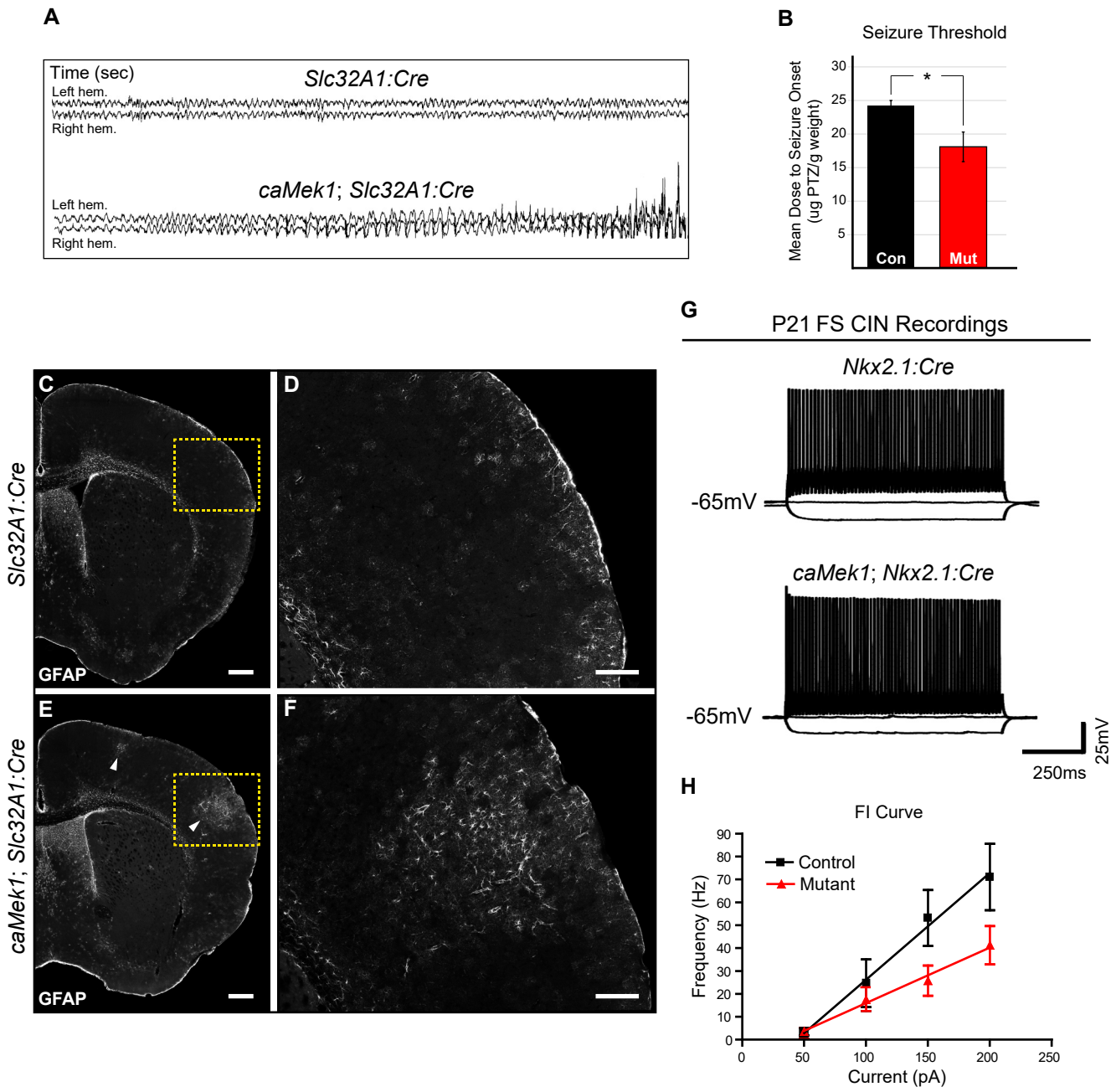

I

Parameter	Control (mean ± SEM)	Mutant (mean ± SEM)	p-value
Resting Membrane Potential (mV)	-67.08 ± 1.090	-66.78 ± 1.245	0.86
Input Resistance (MΩ)	203.3 ± 24.55	296.7 ± 33.47	0.03
FI Slope (Aps/pA)	0.570 ± 0.158	0.165 ± 0.050	0.03
Adaptation Index	0.959 ± 0.147	0.796 ± 0.072	0.39
Rheobase (pA)	117.9 ± 18.96	80.00 ± 13.79	0.14
Action Potential Threshold (mV)	22.33 ± 1.469	22.00 ± 1.106	0.87
Action Potential Amplitude (mV)	65.17 ± 2.229	74.33 ± 2.386	0.01

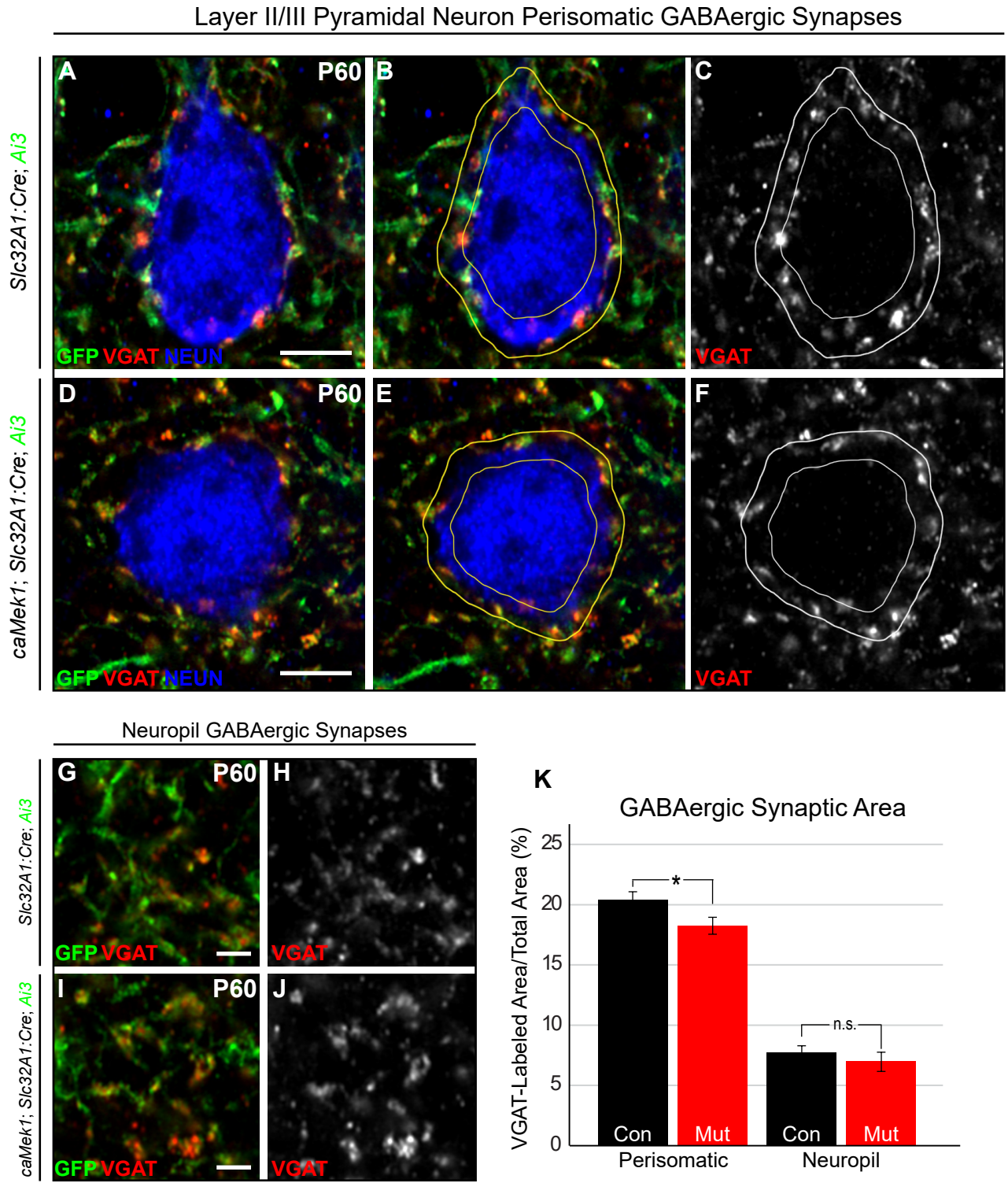

Figure 7

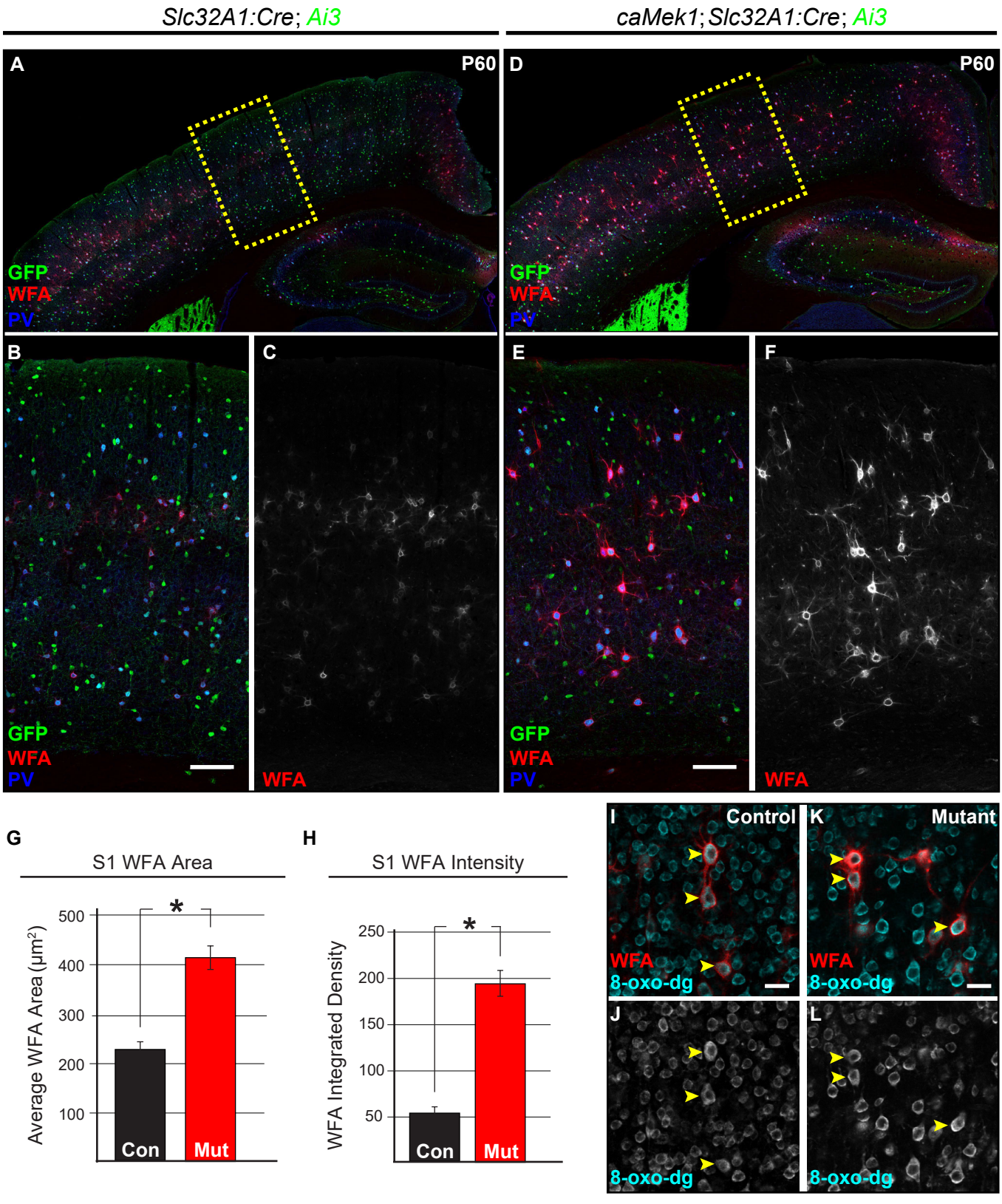

Figure 8

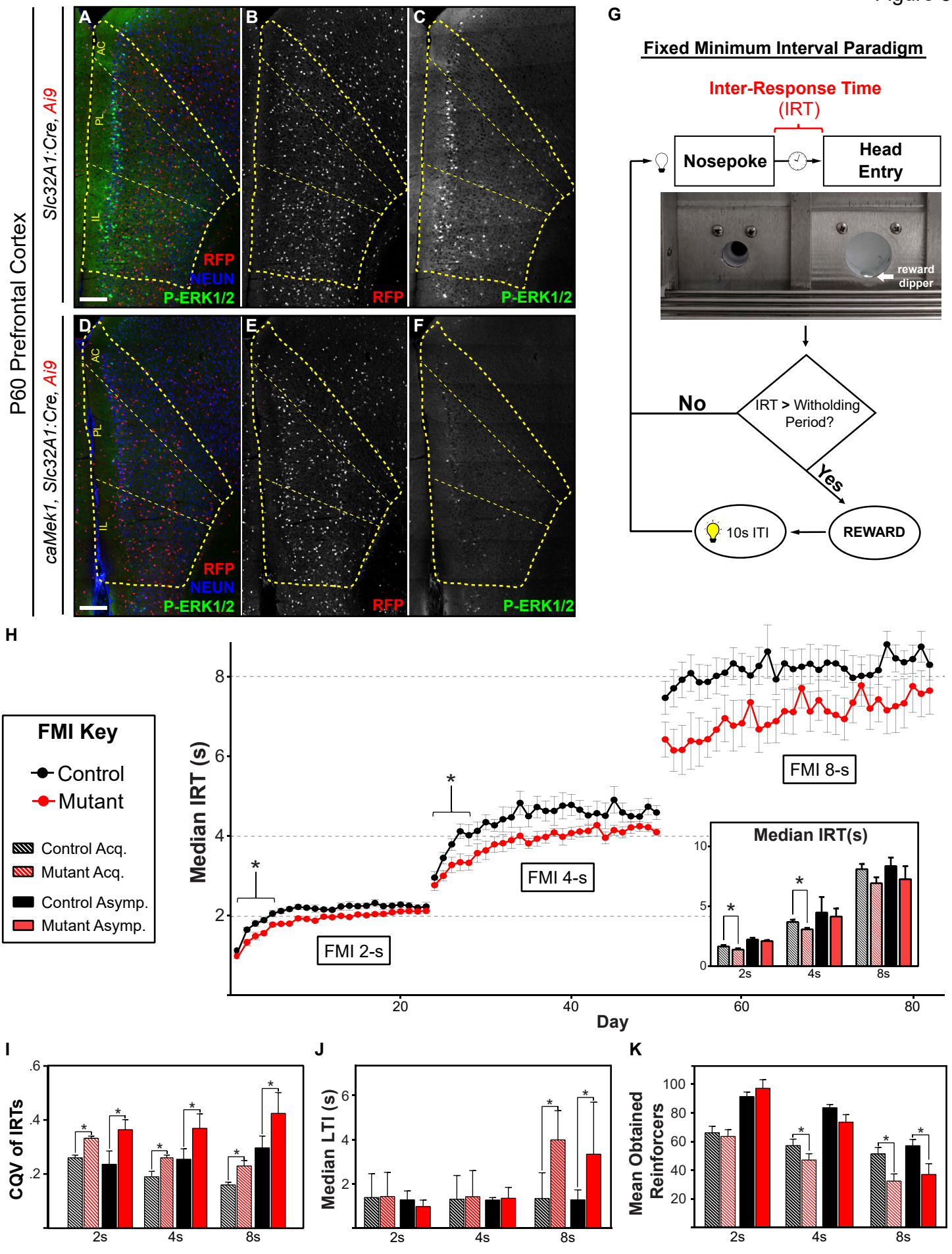

Graphical Abstract